ResearchGate

See discussions, stats, and author profiles for this publication at: https://www.researchgate.net/publication/383098799

Defining an exposure index along the Schleswig-Holstein Baltic Sea coast

Article *in* Marine Geology · August 2024

DOI: 10.1016/j.margeo.2024.107382

CITATIONS
0

READS
27

3 authors, including:

Pushpa Dissanayake
Niedersächsischer Landesbetrieb für Wasserwirtschaft, Küsten- und Naturschutz
67 PUBLICATIONS **880** CITATIONS

SEE PROFILE

Johanna Amft
Leibniz Universität Hannover
4 PUBLICATIONS **12** CITATIONS

SEE PROFILE

All content following this page was uploaded by Pushpa Dissanayake on 23 August 2024.

The user has requested enhancement of the downloaded file.

Defining an exposure index along the Schleswig-Holstein Baltic Sea coast

Pushpa Dissanayake (Corresponding author)

Coastal Research Station, State of Lower Saxony Agency of Water Management, Coastal Defence and Nature Conservation (FSK-NLWKN), Jahnstrasse 1, 26506 Norden, Germany

Formerly, Coastal Geology and Sedimentology, Institute of Geosciences, Kiel University (CAU), Otto-Hahn-Platz 1, 24118 Kiel, Germany

++49(0) 4931 947 198

++44(0) 4931 947 125

pushpa.dissanayake@nlwkn.niedersachsen.de

Johanna Amft

Institute of Statistics, Leibniz University Hannover, Königsworther Platz 1, 30167 Hannover, Germany

meier@statistik.uni-hannover.de

Philipp Sibbertsen

Institute of Statistics, Leibniz University Hannover, Königsworther Platz 1, 30167 Hannover, Germany

sibbertsen@statistik.uni-hannover.de

https://doi.org/10.1016/j.margeo.2024.107382

Abstract

A wind exposure index (EI), which indicates the main physical driver of a coastal system, was developed along the Schleswig-Holstein Baltic Sea (SH) coast – Germany, to demonstrate the highly dynamic coastal stretches (i.e., potential erosion hotspots). The approach used three steps to define more accurate EIs. Initially, a representative wind year (RWY), which has similar physical characteristics as in the long-term data, was defined by analysing measured wind data from 2000 to 2019 at four stations distributed in the entire area of interest. The RWY was identified by a statistical comparison of wind speeds in 5 classes and 36 directional sectors between summer to summer yearly wind and the overall data. The selected RWY spanned from 01.09.2016 to 31.08.2017 and showed a reasonable agreement with the overall data (*Skill* = 0.77 and *rmsd* = 0.56 m/s). Next, high spatiotemporal nearshore hydrodynamics over the RWY were predicted using a model nesting approach of two domains in Delft3D. The predicted nearshore hydrodynamics indicated fair agreements with the measured data (R^2: 0.87 – 0.90 for water levels and 0.75 – 0.86 for wave heights). Finally, the predicted water level and wave height time series in the nearshore area (~ 5 m MSL depth) were used for the analysis of the EI adopting a 2-step procedure capturing short- and long-term correlations as well as seasonal long-range dependencies of the time series. This approach allows to model the clustering behaviour of extreme values of both parameters and provides reasonable EIs along the SH coast. The exposed areas display high EIs (e.g., 1 at the east of Fehmarn), while sheltered areas and bays have low values (e.g., 0 at Eckernförde Bay). The higher the EI the stronger the coastal dynamics and thus strong erosion can be expected. Interestingly, the EI varies considerably even along the exposed coastal stretches with long fetches, which indicates the sensitivity of the EI to the local morphology, which determines the nearshore hydrodynamics. Therefore, a definition of the EI based on nearshore hydrodynamics provides an accurate index of local physical drivers of a coastal system. The developed approach can be adopted to any coast, and provides useful information on the potential erosion areas for the coastal managers.

Key words: *representative wind year, numerical modelling; Delft3D, nearshore hydrodynamics, statistical analysis; GARMA-POT, GPD, IID, Baysian-Information-Criterion*

1. Introduction

Wind exposure is a key physical driver in coastal systems and large lake environments defining the accommodating habitat types and the shoreline characteristics (Mason et al., 2018; Mann and Lazier, 2013; Minns and Wichert, 2005; Burton et al., 2004). Habitat types depend on the exposure of the coast, e.g., suitability for specific plant, fish species (Randall et al., 1996; Zarski et al., 2004), and thus influencing on the coastal ecosystems. Wind exposure affects on the coastal morphology by shoreline erosion rates, sediment sorting and resuspension (Marsh and Marsh, 1987; Schwab et al., 2000). In the offshore area, the basin scale processes (e.g., thermal stratification, upwelling/downwelling) are governed by wind exposure (Yurista et al., 2016; Plattner et al., 2006). In a semi-enclosed system, such as the Baltic Sea, different wind pattern and complex topo-bathymetry surrounded by islands drive entirely the nearshore hydrodynamics (Soomere, 2023). The severity of hydrodynamics is well replicated by the occurrence of water levels and wave heights, which drive local currents determining sediment transport and thus morphological state of the coast (Dissanayake et al., 2021a). Therefore, an attempt to combine wave heights and water levels representing nearshore hydrodynamics would provide a more specific index to quantify the effect of wind exposure for a particular stretch of this coast.

Wind exposure is commonly measured as fetch, i.e., the distance over which wind can travel across open water (Mason et al., 2018). Several methods are employed for estimating fetch in systems like the Baltic Sea. A simple approach calculates direct fetch from the dimensions of the water body (maximum length, length and width, surface area) (Klaff, 2002; Håkanson, 1981). This approach has been improved by averaging the fetch over several wind directions, which accounts for the dominant variations of the wind patterns, so called effective fetch (Håkanson, 1981). The effective fetch was further expanded by Keddy (1982), in which a relative exposure index was developed by incorporating both wind speed and direction. In contrast to these approaches, we develop a spatially discrete variable along the Baltic Sea coast, exposure index (EI), by statistically optimising the predicted water levels and wave heights of numerical modelling to provide a more accurate indicator of the influence of wind exposure in the nearshore hydrodynamics, which affect on the physical setup of the coast.

Numerical modelling studies in the Baltic Sea have mainly investigated large-scale hydrodynamic processes (e.g., Soomere, 2023; Brünning et al., 2018; Gräwe and Burchard, 2012). Soomere (2023) provided a review of different approaches of wave modelling, advancements, inter-comparisons and future need of improvements, and their suitability of applications. He further emphasized the requirement of high-quality wind fields though there are sophisticated models. The effect of fetch on wave generation and propagation is a main phenomenon of these numerical models in estimating hydrodynamics. Brünning et al. (2018) presented an operational numerical model (BSH-HBM) combining the North Sea and the Baltic Sea together, which provides several physical parameters (e.g., water level, current, wave height, surface temperature). In the case of the Baltic Sea, it is highlighted that input of correct basin-scale oscillations (seiches) and wind fields is of importance to predict more accurate parameter values. Occurrence of storm surges for present and future scenarios was simulated in the western part of the Baltic Sea by Gräwe and Burchard (2012). For the future scenarios, they found an increase of mean wind speed approximately by 4%, and the sensitivity analysis by increasing wind speed leads to high surge levels. These example large-scale studies disclosed that wind is the main governing parameter for the Baltic Sea dynamics. In our modelling approach, we used a model nesting approach to downscale large-scale forcing to the local scale, i.e., the SH coast. The largest domain was simulated with the forcing obtained from the Baltic Sea Scale model of Gräwe et al. (2015). Such approach enables to predict the nearshore hydrodynamics in high spatiotemporal resolutions along the SH coast starting with the large-scale forcing.

Statistical modelling is commonly used to analyse the occurrence of extreme events following the popular Peak-Over-Threshold (POT) approach (Davison and Smith, 1990) in coastal (e.g., Bernardara et al., 2011; Dissanayake et al., 2021a,b) and ocean (e.g., Méndez et al., 2006; Cañellas et al., 2007) engineering applications. However, in the case of cyclical behaviour and strong dependence structures in the underlying time series, as expected in the Baltic Sea, the standard POT model faces the problem of strong clustering effects of the extremes. To address this complication, a novel two-step procedure which is based on the approach in Dissanayake et al. (2021b) is herein developed. The first step estimates the cyclical structure and models the dependence structure in the data. Filtering the data by the estimated effects results in independently and identically distributed (*iid*) residuals. To these residuals, we apply in the second step the standard POT model, for which the threshold parameter is estimated by using the automatic threshold selection procedure of Thompson et al. (2009). This procedure provides POT quantiles for the *iid* residual series. To obtain interpretable quantiles for the original series, the respective quantiles for our original data is computed thus taking cycles and dependence structures into account.

The main objective of our study is to define a high spatial resolution index (EI), which is governed by the local physical processes along the coast of Schleswig-Holstein Baltic Sea (SH) in Germany, to indicate the severity of the wind exposure. Our main motivation is to identify the highly dynamic coastal stretches (i.e., potential erosion hotspots), which demand high management interventions. Our approach uses numerical modelling to develop high spatiotemporal hydrodynamics along the coast and statistical modelling to derive the EI combining the variations of water levels and wave heights. Our main hypothesis is, even at the coastal stretches with long fetches, there could be considerable variations of the EI depending on the nearshore morphology, which drives the local hydrodynamics. Therefore, a definition of the EI using nearshore hydrodynamics provides more accurate status of a coast rather than an estimation of EI using fetch lengths and wind parameters.

To achieve the main objective, the performed work is presented in the following sequence. Section 2 describes the study area and the collected field data. The study approach is elaborated in section 3, and the results are given in section 4. In section 5, our results are discussed with the previous studies. Section 6 provides the conclusions of this study.

2. Study area and field data

2.1 Study area

Study area is the Schleswig-Holstein Baltic Sea (SH) coast, which spans from Flensburg to Travemünde of the German Blatic Sea coast (Figure 1a). This coastal stretch has a length of about 399 km (mainland: 328 km and Fehmarn Island: 71 km), and consists of different geomorphological features varying from sandy beaches, coastal lowlands to cliff coasts (Averes et al., 2021). These features are evidence of the deposition of glacial and interstadial sediment processes during the Pleistocene (Dreimanis and Lundqvist, 1984). The Pleistocene deposits were increasingly affected by marine forces with the Holocene sea level rise (Fleming et al., 1998). Therefore, the present-day formation of the coastline is a result of erosion, material transport and deposition processes. Cliff erosion largely contributes to the littoral sediment budget (Averes et al., 2021). The active cliffs (i.e., with the influence of marine hydrodynamic forces) represents about 85 km (~20%) of the coastline (LKN-SH, 2023). In the last century, the cliff retreat occurred averaged annual rate of about 0.2 m/year (Ziegler and Heyen, 2005). Bed sediment composition of the nearshore area has a very wide grain-size spectrum consisting of silt/clay, sand, pebbles and boulders (Ehlers, 2020).

Environmental forcing along the SH coast varies from Flensburg to Travemünde depending on the local coastline orientations and the prevailing morphological features. Water level oscillation of this micro-tidal coast is mainly governed by the occurrence of seiches, which has a period of more than a day in the western part of the Baltic Sea (Metzner et al., 2000). The minimum and maximum water levels reached during the analysis period (2016 - 2017) are about -0.9 m and 1.6 m respectively, while astronomical tidal range is about 0.2 m at S3 (see Figure 2). However, Dissanayake et al. (2022) showed that the micro-tidal contribution to water levels has an important role in sediment transport along this coast. Locally generated sea waves dominate based on the predominant fetch length, while swell contribution is negligible (Mason et al., 2018). The coastal stretches facing to the NE direction deserve for long fetch lengths. The major dynamics in the Baltic Sea are governed by the wind driven processes (Soomere, 2023). Dominant wind approach is within the sector from SW-NW. However, extreme events (wind magnitude > 15 m/s) occurred during the analysis period from the N-NE sector (LKN-SH). Such events can result in average velocity pattern towards west along the coast, though the dominant wind approach favours it towards east, and so does the sediment transport (Dissanayake et al., 2022).

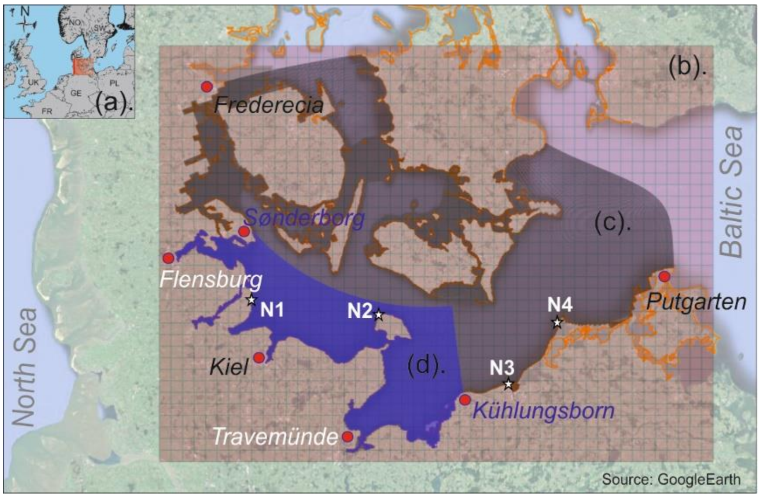

Figure 1. Location of Schleswig-Holstein (SH) Baltic Sea coast, Germany (a), Spatial wind-data grid from German Weather Service (DWD) (https://opendata.dwd.de) (b), SH model grid enclosing the coast from Frederecia (Denmark) to Puttgarten (Germany) (c), and SHC model grid spanning from Sønderborg (Denmark) to Kühlungsborn (Germany) covering the entire SH coast from Flensburg to Travemünde (d), and the selected wind measuring stations operated by DWD: N1 (Schönhagen), N2 (Fehmarn), N3 (Warnemünde) and N4 (Darss). Orange-line indicates the coastline from European Environmental Agency (https://www.eea.europa.eu).

2.2 Field data

For this investigation, water levels, wave characteristics, bathymetry data and coastline were collected from different sources covering the analysis period, together with the long-term measured wind data along the SH coast and the forecasted spatiotemporal wind fields.

Long-term measured wind data was collected from German Weather Service (DWD: https://opendata.dwd.de) for four stations, which are distributed along the SH model domain (see locations N1 – N4 in Figure 1), to define a representative wind year. The data set has a 10 minutes resolution and different coverage depending on the station, i.e., Schönhagen (N1): 1995 – 2019, Fehmarn (N2): 1996 – 2019, Warnemünde (N3): 1992 – 2019 and Darss (N4): 2000 – 2019. The forecasted spatiotemporal wind fields were obtained from DWD for the period of 2016 – 2017 to drive the numerical simulations. These data are based on the COSMO (COnsortium for Small-scale MOdelling) reanalysis with temporal and spatial resolutions 1 h and 6 km × 6 km respectively. For the same period, measured water levels and wave characteristics were collected from the Federal Maritime and Hydrography Agency (BSH). Water level data were collected from six stations from Flensburg to Travemünde (see S1 – S6 in Figure 2), and wave characteristics were employed from three buoy locations (see W1 – W3 in Figure 2). Water level data has a 1 minute resolution at all stations, while the wave buoy at W1 (LTKiel, Figure 2) provides 1 h resolution of data, and that of W2 (Schoenbeg-Coast) and W3 (Schoenberg-Nearshore) is 10 minutes. These data were used for the model calibration and validation. For the forcing at the open boundaries of the SH model (Figure 1c), spatiotemporal water levels (resolution 1 h) were obtained from the Baltic Sea scale model (Gräwe et al., 2015). The model bathymetries were set up using two sources of data. For the nearshore area, the high resolution BSH data (50 m × 50 m), which covers the German Baltic Sea coast, was used, while the offshore bathymetry is based on the coarse resolution data (660 m × 750 m) from the Baltic Sea research institute Warnemünde (IOW), Germany. The nearshore area consists of shallow planes (see SHC bathymetry in Figure 2). To set up the model domains, the coastline, which was obtained from European Environmental Agency (EEA: https://www.eea.europa.eu), was followed. For the analysis of nearshore hydrodynamics, model predicted water levels and wave heights were monitored at the coastal points, which are located around 5 m depth with 500 m spacings along the entire SH coast. These points were defined based on the existing coastal reference points from the Schleswig-Holstein coastal agency (LKN-SH), which are spaced by 50 m along the coast. The total number of 500 m spacing points counts 675 following the local variations of the coastline.

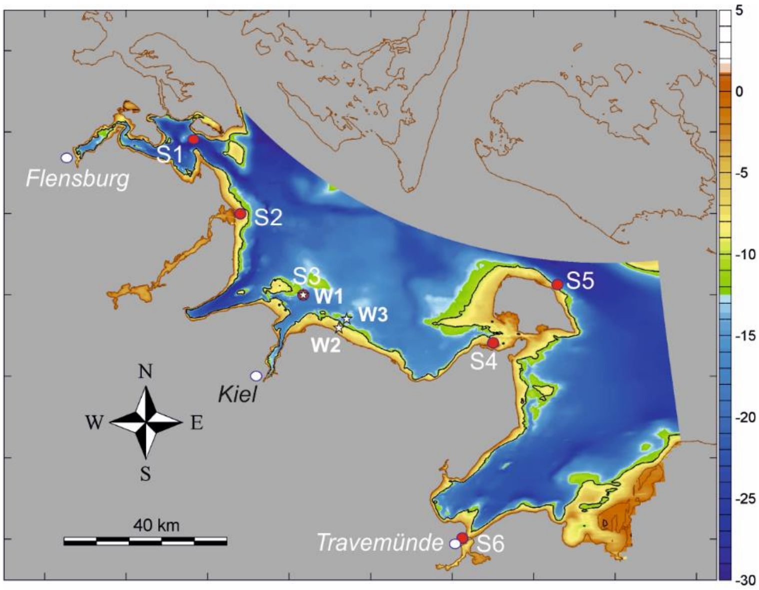

Figure 2 SHC model bathymetry constructed using BSH (https://www.geoseaportal.de) and IOW (https://www.io-warnemuende.de/topography-of-the-baltic-sea.html) bathymetry data. Colour indicates water depths. Water level measuring stations are indicated with S1 (LTKalkgrund), S2 (SchleimündeSP), S3 (LTKiel), S4 (Heiligenhafen), S5 (Marienleuchte) and S6 (Tavemünde), and wave buoy locations are shown with W1 (LTKiel), W2 (Schoenberg - Coast) and W3 (Schoenberg - Nearshore). Orange-line indicates the coastline from EEA (https://www.eea.europa.eu).

3. Approach

Our approach is based on the occurrence of wind, which is the main driver for hydrodynamics, and in turn sediment transport and morphodynamics in the micro-tidal Baltic Sea (Soomere, 2023).

To classify an accurate physical index considering long-term wind data and nearshore hydrodynamics, there are three steps in the analysis, (1) Defining a representative wind year for the model simulations, (2) Numerical modelling to develop nearshore water level and wave height variations, and (3) Statistical modelling to derive an exposure index (EI) along the SH coast.

3.1 Representative Wind Year (RWY)

To define a general EI, the analysis needs to be carried out covering a large data set. This requirement was circumnavigated by estimating a RWY, which has similar characteristics to the long-term wind data set.

The measured long-term wind data from four DWD stations (https://opendata.dwd.de), which are distributed along the coast of the SH domain, were selected for this analysis (see locations in Figure 1). As mentioned earlier, the temporal coverages of the data sets vary depending on the station. Therefore, the data from a common coverage from 2000 to 2019 was used to analyse a representative wind year.

Initially, wind years were defined from summer to summer considering adjacent years (e.g., from 01 September 2000 to 31 August 2001, from 01 September 2001 to 31 August 2002 and so on). Then, the probability of occurrence of wind speeds was binned considering 6 wind speed classes (*m*) with 5 m/s intervals (0-5, 5-10, …., 25-30) and 36 directional classes (*n*) with 10^{o} intervals (i.e., 0-10, 10-20, …, 350-360). For each bin, the probability (*p*) was estimated using Eq. 1.

$$p_{i,j} = \frac{\{S(S_{i-1,j}<S\leq S_{i,j} || D_{i-1,j}<D\leq D_{i,j})\}}{\{S\}} \qquad (1)$$

where, *S* is wind speed (m/s), and $i \rightarrow 1{:}m$, $j \rightarrow 1{:}n$

Next, a representative wind speed for each bin (*a*) was evaluated considering the respective wind events and the probability of occurrence using Eq. 2.

$$a_{i,j} = \frac{p_{i,j}\sum_{q=1}^{k} S_q}{k p_{i,j}} \qquad (2)$$

where, *k* is number of wind events in a bin

Along the SH coast, wind approach determines the prevailing fetch length, and hence wave heights. Therefore, a representative wind speed for each directional class (*rs*) was finally estimated using the respective binned representative wind speed (*a*) and the probability of occurrence (*p*) as in Eq. 3.

$$rs_j = \frac{(p_{i,j}a_{i,j}+p_{i+1,j}a_{i+1,j}+p_{i+2,j}a_{i+2,j}+\cdots+p_{m-1,j}a_{m-1,j}+p_{m,j}a_{m,j})}{\sum_{i=1}^{m} p_{i,j}} \qquad (3)$$

This procedure was repeated for each wind year ($rs_{j,y}$) and for the overall wind climate from 2000 to 2019 ($rs_{j,o}$). By comparing $rs_{j,y}$ and $rs_{j,o}$ using statistical parameters (see 3.4), the best representative yearly wind climate for the overall wind data from 2000 to 2019 was defined as RWY.

3.2 Numerical modelling

The aim of numerical modelling is to develop high spatiotemporal water levels and wave heights representing nearshore hydrodynamics along the SH coast, which are difficult to obtain from the field measurements. The Delft3D modelling suite was herein employed to simulate the nearshore hydrodynamics. After model calibration and validation against the available field measurements, the nearshore hydrodynamics were simulated over the RWY and the predicted water level and wave height variations (i.e., 10 minutes intervals) were extracted at the predefined 500 m spacing coastal points (see 2.2) representing the high spatiotemporal data to derive the EI.

3.2.1 Delft3D Modelling suite

Delft3D is an open-source three-dimensional model based on a finite difference approach (Lesser et al., 2004; Stelling, 1984; Stelling and Lendertse, 1991), and has shown skill in simulating nearshore hydrodynamics for a wide range of case studies (e.g., Hunt et al., 2017, Van Ormondt et al., 2020; Dissanayake and Winter, 2020). In the present analysis, a depth-averaged approach (2DH) was used. The wave dynamics were simulated by online wave coupling with the wave model, SWAN (Booij et al., 1999), which allows simulating wave–current interactions at a specified time interval. A 1 h interval was used to capture the tidal variation, and the temporal resolution of the wind (1 h). Waves are exclusively internally generated within the model domains (see 3.2.2). Water level variation from micro-tidal contribution and seiches in the Baltic Sea plays an important role in estimating hydrodynamics (Dissanayake et al., 2022). Therefore, including wave–current interactions is a prerequisite to accurately simulate the nearshore hydrodynamics.

3.2.2 Model domains and boundary forcing

A nested modelling approach was used to downscale the large-scale forcing (SH, see in Figure 1) to the local-scale high resolution simulations (SHC). The SH domain has the maximum grid resolution at the coast of 300 m × 500 m (cross- × alongshore), while it is 75 m × 125 m in SHC. Bathymetries of both domains were prepared by combining the high resolution BSH data and the coarse resolution IOW data (see SHC model bathymetry in Figure 2). Each domain consists of two open boundaries (SH: east and west, SHC: east and north). The SH model was first simulated applying spatiotemporal water levels at the east and the west boundaries, and online-coupling with waves. These water levels are embedded with local (wind, wave) and large (tide, seiches) scale oscillations. Using the predicted results of SH, boundary forcing for the SHC model was established (east: currents and north: water levels). Then, the SHC model was simulated forcing with these boundaries together with the wave-current interaction, which was set up by online-coupling with SH. It should be noted that the wave boundary of the SH model was set to dummy values as there is no influence from boundary waves to the waves in the area of interest according to our initial sensitivity analyses.

3.2.3 Simulations

Initial simulations were carried out for calibration (M1 – M7) and validation (V1 – V2 in Table 1), and thereafter the model was simulated for the RWY. The calibration simulations spanned for the period of January 2016 applying different bed roughness schemes: spatial constant (M1 – M5) and spatial varying (M6 – M7) Chézy values. Using the calibrated model, the validation was performed by simulating the model for two independent periods: September 2016 and January 2017. The model covering the RWY was finally simulated to monitor the nearshore water level and wave height variations.

Simulation		**Bed roughness scheme**	**Period**
Calibration	M1	Chézy (*C*): 40 $m^{1/2}/s$	January 2016
	M2	Chézy (*C*): 50 $m^{1/2}/s$	
	M3	Chézy (*C*): 60 $m^{1/2}/s$	
	M4	Chézy (*C*): 65 $m^{1/2}/s$	
	M5	Chézy (*C*): 70 $m^{1/2}/s$	
	M6	Manning (*n*): 0.022 $s/m^{1/3}$	
	M7	Manning (*n*): 0.025 $s/m^{1/3}$	
Validation	V1	M2	September 2016
	V2	M2	January 2017
Representative wind year (RWY)		M2	01 September 2016 – 31 August 2017

Table 1 Simulations undertaken for calibration using different bed roughness schemes (Spatial constant M1 – M5: *C* and Spatial varying M6 – M7: $C=\sqrt[6]{H}/n$, where *H* (m) is water depth) and validation, and for the representative wind year (RWY) to monitor nearshore hydrodynamics

The SH domain was simulated applying a time step (Δt) of 5 minutes and a spin-up period of 3 days. Hydrodynamic simulation over the RWY took about 3.5 days using 60 nodes in the CAU HPC cluster (CAU: Christian-Albrechts-Universität zu Kiel). The SHC domain was simulated applying a Δt of 1 minute, and took 31 days to simulate hydrodynamics over the

RWY using 64 nodes in the cluster. It should be noted that the optimised number of nodes were selected through sensitivity analyses.

3.3 Statistical analysis

Occurrence of water levels and wave heights determines the severity of nearshore hydrodynamics, which drive sediment transport and in turn morphological changes (Dissanayake et al., 2021a). This is particularly applicable for the SH coast as both these physical parameters are dominated by wind. Therefore, the predicted high spatiotemporal water levels and wave heights (3.2) are hereon employed in the statistical analysis to estimate an accurate EI.

The derivation of the EI uses a 2-step generalized autoregressive moving average (GARMA)-POT model (POT: Peak-Over-Threshold), generalizing the approach of Dissanayake et al. (2021a,b) for non-cyclical data. Applying a POT method uses the fact that exceedances of a threshold converge to a Generalized-Pareto-Distribution (GPD) for independent and identically distributed observation. In our situation, this is not the case as the data is highly cyclical and persistent. Therefore, the exceedances over a threshold are subjected to clustering effects and thus the POT model is no longer applicable. We therefore have to pre-filter the data to obtain independent and identically distributed residuals, which eliminate the exceedance clusters and allow application of the POT model. Our approach is twofold. The first step models the cycles and dependence structure of the data by fitting the k-factor GARMA of Giraitis and Leipus (1995) and Woodward et al. (1998). This model generalizes the autoregressive fractionally integrated moving average (ARFIMA)-model for strongly dependent data by allowing for cyclical long memory. In the second step, the POT model is applied to the data.

3.3.1 Step 1 - k-factor GARMA

Cyclical long-range dependence can be regarded as an intermediate case between a short-range dependent cyclical process and a cyclically integrated model. We focus on the k-factor GARMA model (GARMA-k), which was proposed by Gray et al. (1989) and generalised by Giraitis and Leipus (1995) and Woodward et al. (1998). This type of model represents a generalisation of ARFIMA processes since it allows for poles in the spectral density at arbitrary frequencies instead of the zero frequency alone. Therefore, the GARMA-k process can model different degrees of long-range dependence at any desired periodic frequency.

Assuming that Y_t is zero-mean white noise with variance σ_u^2 , the k-factor GARMA model is given by

$$\Phi(L)\prod_{a=1}^{k}(1-2\cos\gamma_a L + L^2)^{d_a} X_t = \Theta(L)Y_t \tag{4}$$

where, $$\Phi(L) = 1-\phi_1 L - \cdots - \phi_p L^p$$

$$\Theta(L) = 1-\theta_1 L - \cdots - \theta_q L^q$$

with p and q being non-negative integers, d_a representing the memory parameter associated with the a^{th}cyclical frequency γ_a, and L denoting the lag operator such that $LX_t = X_{t-1}$.

In order to fit the GARMA-*k* model to the wave height and water level variations along the SH coast, the model order *k* needs to be determined. We utilise the automatic model order selection procedure of Leschinski and Sibbertsen (2019), which is based on iterative filtering and periodogram based tests for persistent cyclical behaviour in time series. The underlying idea of the procedure is that the residuals from a correctly specified Gegenbauer model should exhibit no pole in the periodogram. If the periodogram of a filtered process is still characterised by poles, the model order is not sufficient and needs to be increased. For their procedure, Leschinski and Sibbertsen (2019) propose a test for the null hypothesis of a bounded spectral density against the alternative of at least one pole at an unknown frequency. This test is applied following every filtering iteration in order to determine whether the residual process still contains significant persistent periodicity. After choosing the appropriate cyclical long-range dependence dynamics, the ARMA model orders *p* and *q* can be selected using an information criterion when re-estimating the selected model specification via a suitable Whittle likelihood procedure. As information criterion, we use the Bayesian information criterion (BIC).

3.3.2 Step 2 - POT

Having modelled the dependency structure of the time series, the residuals in the step 1 can be regarded as *iid* data. Therefore, we can rely on the standard POT methodology to characterise the behaviour of the high-threshold exceedances in order to infer suitable thresholds for each time series.

For an unknown distribution function F of some random variable Y, we define the conditional distribution function of Y above some threshold u, i.e. the conditional excess distribution function as,

$$F_u = P(Y - u \leq z \mid Y > u) = \frac{F(u+z)-F(u)}{1-F(u)}, \;\; for \;\; 0 \leq z \leq y_F - u \qquad (5)$$

where, y_F represents the (finite or infinite) right end point of the underlying distribution F and z is the size of the excess above the threshold u (Leadbetter, 1991).

According to the Pickands-Balkema-De Haan theorem (Pickands, 1975; Balkema, 1974), the conditional excess distribution function F_u of a sequence of *iid* variables $\{Y_i\}_1^T$ converges for $u \to \infty$ to a generalised Pareto distribution (GPD) with cumulative distribution function (CDF).

$$G_{\xi,\sigma}(z) = \begin{cases} 1 - \left(1 - \xi \frac{z}{\sigma}\right)^{-1/\xi}, \; \xi \neq 0, \\ 1 - exp\left(-\frac{z}{\sigma}\right), \; \xi = 0, \end{cases} \qquad (6)$$

where, ξ is the shape and $\sigma > 0$ the scale parameter

Further, the POT approach may be regarded through the lens of a Marked Point Process (MPP), where an extreme event is defined by its associated occurrence time and mark size. The mark size corresponds to the size of the excess above the threshold previously denoted by z. For a high enough threshold u and assuming that times and mark sizes are independent of each other, the point process of extreme events converges to a marked Poisson process: the extreme events occur at times of a homogeneous Poisson process, while the *iid* mark sizes follow a GPD (Leadbetter, 1991). This process implies that inter-event times are characterised by an *iid* exponential distribution. These limiting distributions can be exploited to obtain diagnostic tools for checking the assumptions of the POT method (see e.g., Embrechts, 2012). For a technical introduction to the MPP representation as well as for the corresponding maximum likelihood estimation is referred to Dissanayake et al. (2021b).

A central question in the POT framework is how to choose a suitable threshold u. The standard approach is based on graphical diagnostics (see e.g., Coles, 2009): the mean residual life plot and parameter stability plots for the estimated GPD. If the GDP provides an appropriate approximation to the excess distribution above some threshold u_0, the mean residual life plot should be roughly linear in u, while the estimates of the shape parameter ξ and the parameterised scale parameter $\sigma^* = \sigma - \xi u$ should be constant. However, for a large number of time series, such a manual approach is infeasible. Therefore, we deploy an automatic threshold selection procedure. For a comprehensive review of existing automatic threshold selection methods, it is referred to Scarrott and MacDonald (2012).

We follow the approach proposed by Thompson et al. (2009): a uniformly spaced grid of potential threshold values between the median and the 99.5% empirical quantile is set. For each possible threshold, a GPD to the resulting exceedances and calculate the differences in the parameterised scale parameters σ^* for neighbouring thresholds is fitted. We expect the scale differences to be centred around zero and to follow an approximate normal distribution if the GPD is a valid model. The sequence of scale differences is then treated as a sample of normal random variables and a forward selection procedure is applied: increasing the threshold increment by increment, we repeatedly perform Pearson's Chi-square test under the assumption of normality with mean zero. If the null hypothesis of normality is not rejected, the current threshold is considered to be consistent with a GPD. However, if the null hypothesis is rejected, we consider the next highest threshold and remove the current scale difference from the sample. We follow the recommendation of Thompson et al. (2009) and perform a size 0.2 Pearson normality tests.

The automatically determined thresholds values u correspond to quantiles in the *iid* GARMA-residuals from the step 1. In order to obtain interpretable thresholds in terms of the original data, computing the quantiles from the step 2 for the original time series is suggested. In this way, the final thresholds are established by considering all short-range, long-range and seasonal dependence, and can be rescaled to an EI with values in [0,1] by the min-max scaling.

3.4 Comparison parameters

The agreement between the overall wind climate from 2000 to 2019 (OW) and the yearly wind climates (YW) was estimated using the following parameters,

Mean Relative difference (μ) indicates mean change between overall (rs_o) and yearly (rs_y) wind climates relative to the overall wind (Eq. 7).

$$\bar{\mu} = \frac{1}{n}\sum_{j=1}^{n} \mu_j = \frac{1}{n}\sum_{j=1}^{n} \frac{(rs_{j,y} - rs_{j,o})}{rs_{j,o}} \qquad (7)$$

Standard deviation (σ) provides the deviation between overall and yearly wind climates with respect to the mean relative difference (Eq. 8).

$$\sigma = \sqrt{\frac{1}{n}\sum_{j=1}^{n}(\mu_j - \bar{\mu})} \qquad (8)$$

Root mean square difference (*rmsd*) estimates the standard deviation of the change between overall and yearly wind climates (Eq. 9).

$$rmsd = \sqrt{\frac{1}{n}\sum_{j=1}^{n}(rs_{j,y} - rs_{j,o})^2} \tag{9}$$

Variance of overall (V_o) *and yearly* (V_y) *wind climates* indicates the spread of wind climates with respect to its mean value (Eq. 10).

$$V_o = \frac{1}{n}\sum_{j=1}^{n}(rs_{j,o} - \overline{rs_{j,o}})^2 \quad V_y = \frac{1}{n}\sum_{j=1}^{n}(rs_{j,y} - \overline{rs_{j,y}})^2 \tag{10}$$

Covariance (CV) estimates the change of overall and yearly wind climates together. A positive CV implies, both are positively related and have the same trend of variation (Eq. 11).

$$CV = \frac{1}{n}\sum_{j=1}^{n}(rs_{j,o} - \overline{rs_{j,o}})(rs_{j,y} - \overline{rs_{j,y}}) \tag{11}$$

Skill score (*skill*) measures the root mean square difference to the standard deviation. A *skill* of 1 indicates perfect agreement between overall and yearly wind climates, 0 means no agreement, and negative values provide a negative trend (Eq. 12).

$$skill = 1 - \frac{rmsd^2}{\sigma^2} \tag{12}$$

Coefficient of determination (R^2) quantifies the fraction of variation of predicted water levels or wave heights with respect to the measured data (Eq. 13).

$$R^2 = \left[\frac{\sum_{r=1}^{s}(w_{md,r} - \overline{w_{md}})(w_{pd,r} - \overline{w_{pd}})}{\sqrt{(w_{md,r} - \overline{w_{md}})(w_{pd,r} - \overline{w_{pd}})}}\right]^2 \tag{13}$$

where, w is water level or wave height. *md* indicates measured and *pd* model predicted values. s is the number of data points.

Complex correlation coefficient (r_c) is used to compare between two vector time series (Kundu, 1975; von Storch and Zwiers, 1999; Bierstedt et al., 2015), and is hereon employed to compare between DWD-measured and COSMO-reanalysis wind data at the four DWD stations (see Figure 1). A two-dimensional vector time series can be represented by a complex number, $wn(t) = U(t) + i\,V(t)$. The complex correlation coefficient is defined as the complex Pearson correlation between the two complex time series (Eq. 14 and 15).

$$r_c = \frac{\langle wn_1^*(t) wn_2(t)\rangle}{\sqrt{\langle wn_1^*(t) wn_1(t)\rangle}\sqrt{\langle wn_2^*(t) wn_2(t)\rangle}} \tag{14}$$

$$r_c = \frac{\langle U_1U_2 + V_1V_2\rangle}{\sqrt{\langle U_1^2 + V_1^2\rangle}\sqrt{\langle U_2^2 + V_2^2\rangle}} + i\,\frac{\langle U_1V_2 - U_2V_1\rangle}{\sqrt{\langle U_1^2 + V_1^2\rangle}\sqrt{\langle U_2^2 + V_2^2\rangle}} \tag{15}$$

where, *wn* is wind vector, * indicates the complex conjugate, *U* and *V* are real and imaginary components, 1 and 2 denote two wind fields: DWD-measured and COSMO-reanalysis.

The agreement between DWD and COSMO wind time series can then be demonstrated by change in average magnitude ($r_{c,mag}$: Eq. 16) and phase ($r_{c,phase}$: Eq. 17).

$$r_{c,mag} = \frac{\sqrt{\langle U_1U_2+V_1V_2\rangle^2+\langle U_1V_2-U_2V_1\rangle^2}}{\sqrt{\langle U_1^2+V_1^2\rangle}\sqrt{\langle U_2^2+V_2^2\rangle}} \tag{16}$$

$$r_{c,phase} = tan^{-1}\left[\frac{\langle U_1V_2-U_2V_1\rangle}{\langle U_1U_2+V_1V_2\rangle}\right] \tag{17}$$

In addition to R^2 and *rmse* (similar in *rmsd*), *scatter index* and *relative bias* were used to indicate the agreements between measured and predicted water levels and wave heights.

Scatter index (*SCI*) is a relative measure of the scatter between the measured and the predicted water level or wave height. The error is normalised with the maximum of the root mean square (*rms*) of the measured data or its absolute value of the mean (Eq. 18).

$$SCI = \frac{rms_{md-pd}}{\max(rms_{md}, |\langle md\rangle|)} \tag{18}$$

Relative Bias (*RBI*) estimates the relative bias of the predicted values, and it is normalised similar to *SCI* (Eq. 19).

$$RBI = \frac{\langle md-pd\rangle}{\max(rms_{md}, |\langle md\rangle|)} \tag{19}$$

4. Results

4.1 Representative Wind Year (RWY)

The variation of the analysed statistical parameters between overall (OW) and yearly (from 01 September to the adjacent year 31 August) (YW) wind climates are shown in Figure 3 for the summer to summer periods. All parameters denote that Schönhagen has a different pattern compared with the others. This could be due to the fact that the dominant wind at Schönhagen approaches from land (i.e., SW-NW sector), while that of other stations from water (see coastlines and wind roses at all stations in Figure A1). A positive mean relative difference indicates that the YW is higher than the OW and vice versa, and a good agreement has a value close to zero (a). Considering all four stations, the year 2016-2017 has the minimum value, while the maximum negative and positive values correspond to the year 2005-2006 and 2006-2007 respectively. According to the standard deviation derived using the mean relative difference, the first three stations show the minimum value at the year 2003-2004, while the value at Schönhagen is higher than those of others (b). All stations tend to show the maximum deviation at the year 2009-2010. The minimum root mean square difference is shown with the year 2003-2004 (c), while the maximum is in 2009-2010. Difference among stations appear to be higher compared with the previous two parameters. The YWs of Darss have the highest variance with respect to its OW and the lowest is found at Schönhagen (d). Furthermore, it implies that occurrence of wind variability increases along the coast from Schöhagen to Darss (see dash-lines). All stations have positive covariance indicating same trends of variations of the YWs as in the OWs (e). The lower values of the stations are generally shown in year 2005-2006, and the higher in 2016-2017 than the other years. The highest skill score considering all stations is shown in year 2016-2017 (f). In the year 2006-2007, the YW has a strong disagreement with the OW. All stations tend to show lower values in the year 2005-2006 than others.

Each statistical parameter captured different properties of the YW and the OW resulting to different variations along the summer-summer periods. Considering all parameters and the variations at all stations, three YWs were defined as weak, representative and strong. The weak wind year (01 September 2005 – 31 August 2006) has generally low wind speeds compared with that of the overall, while the strong wind year (01 September 2006 – 31 August 2007) has higher wind speeds than the overall. The RWY (01 September 2016 – 31 August 2017) indicates similar characteristics as those in the overall wind climate.

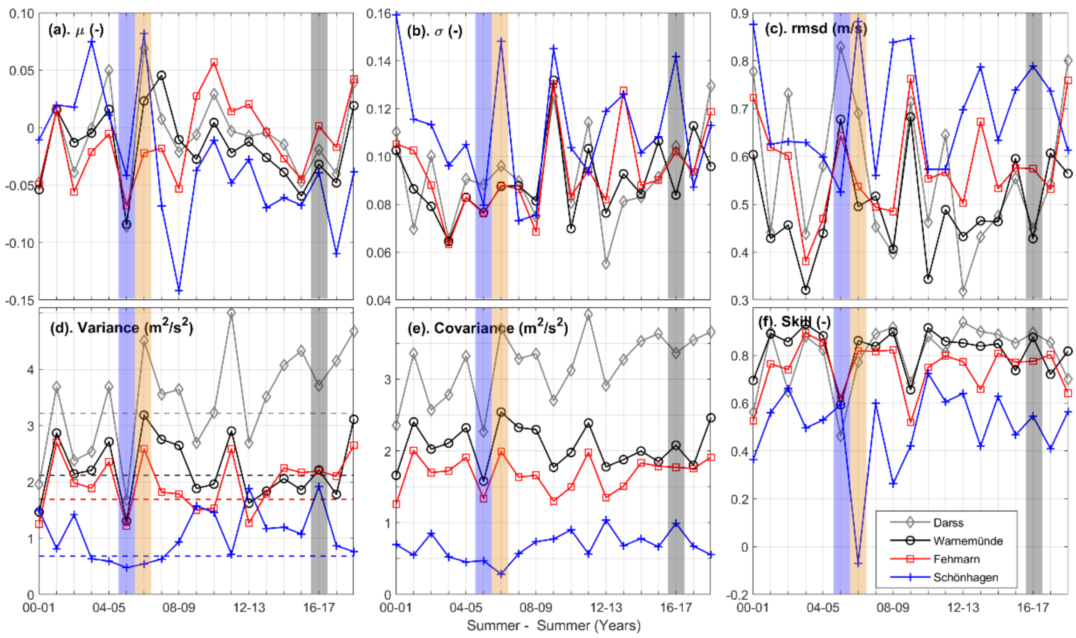

Figure 3 Comparison of the entire 20-year wind climate from 2000 to 2019 (OW) and each summer – summer wind year (YW) using different statistical parameters: Mean relative difference (a), Standard deviation (b), Root mean square difference (c), Variance of OW (dash-line) and YW (solid-line) (d), Covariance between OW and YW (e) and Skill score (f). Defined weak, representative and strong wind years are indicated by blue, gray and orange bars respectively.

Results of the statistical analysis is summarised in Table 2. Accordingly, the RWY shows the best agreement with the OW, and weak and strong wind years indicate considerable deviations at all stations.

Station	(a). μ (-)			(b). Σ (-)			(c). Rmsd (m/s)			(d). Variance (m^2/s^2)			(e). Covariance (m^2/s^2)			(f). Skill (-)		
	Weak	Repres.	Strong	Weak	Repres.	Strong	Weak	Repres.	Strong	Weak	Repres.	Strong	Weak	Repres.	Strong	Weak	Repres.	Strong
Darss	-0.09	-0.02	0.07	0.09	0.10	0.10	0.83	0.45	0.69	-1.54	3.71	4.51	2.27	3.36	3.70	0.46	0.89	0.77
Warnemünde	-0.08	-0.03	0.02	0.08	0.08	0.09	0.68	0.43	0.50	-0.81	0.09	1.07	1.58	2.08	2.54	0.59	0.88	0.86
Fehmarn	-0.07	0.00	-0.02	0.08	0.10	0.09	0.64	0.57	0.54	-0.47	0.51	0.90	1.34	1.77	1.99	0.62	0.77	0.82
Schönhagen	-0.04	-0.04	0.08	0.08	0.14	0.15	0.53	0.79	0.88	-0.20	1.24	-0.14	0.47	0.99	0.28	0.59	0.55	-0.07
Mean value	**-0.07**	**-0.02**	**0.04**	**0.08**	**0.11**	**0.10**	**0.67**	**0.56**	**0.65**	**-0.76**	**1.39**	**1.58**	**1.41**	**2.05**	**2.13**	**0.57**	**0.77**	**0.60**

Table 2 Estimated values of different statistical parameters for the selected Weak, Representative and Strong wind years at the four wind measuring stations: Darss, Warnemünde, Fehmarn and Schönhagen

These defined three wind years (weak, representative and strong) were further compared with the wind roses of the OW at the four stations (see Annex A1). Accordingly, the wind rose of the weak year indicates low wind speeds, though the directions seem to fairly agree with the overall. Apparently, the strong wind year has higher wind speeds than the overall. The wind rose of the RWY has the similar characteristics in wind speed as well as direction as in the overall. Therefore, this wind period, RWY, was used to simulate the models and to monitor high spatiotemporal nearshore hydrodynamics.

For the model forcing, spatiotemporal wind fields (COSMO) were employed over the RWY. Therefore, a comparison was first performed at the four wind stations between the measured (DWD) and the derived wind data from the spatiotemporal wind fields. Magnitude and phase of the complex correlation coefficient indicate a good agreement of these two sources of wind vectors at the four measuring stations (Figure A2). Magnitudes of the stations have values around 0.95 and the phase difference is generally lower than 10^o though Schönhagen shows the maximum difference of about 12^o. Therefore, the COSMO wind data has the similar characteristics as in the measured DWD wind data, and can be used to drive the model simulations.

4.2 Numerical Modelling

4.2.1 Model calibration and validation

Statistical agreements between the measured and the predicted water levels are shown in Figure 4 (a - d) for the calibration simulations applying different bed roughness schemes. The mean value of all 6 stations (red line) has the similar trend of variation to that of the station

LTKiel (blue line: as an exemplary location) (see all locations in Figure 2), though the values are different. This implies that all stations responded to the bed roughness schemes in similar pattern. Both R^2 (a) and *RMSE* (b) indicate the highest and the lowest values for the M2 model (Chézy: 50 $m^{1/2}/s$, see Table 1). *SCI* (c) decreases for the spatial constant roughness schemes (M1-M5), and then increases for the last two spatial varying schemes (M6 and M7). The range of change in all roughness schemes is well under 3%. RBI continuously decreases from M1 to M7. The predictions of the M2 model result in about 9% while the lowest is about 6% (M7). Considering the variations of all statistical parameters, the model setting of M2 was adopted as the calibrated parameters.

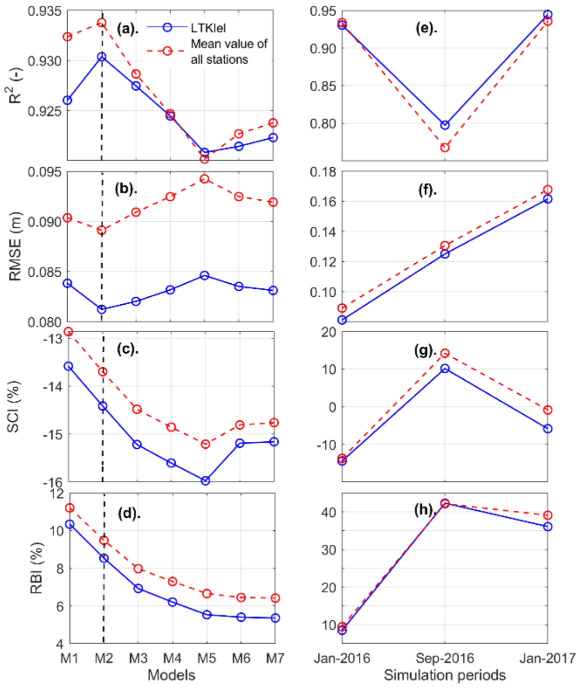

Figure 4 Statistical comparison of measured and calibrated water levels (a) – (d), and validation of model predictions (e) – (h) for three independent periods (January 2016, September 2016 and January 2017). Blue line indicates values comparing measured and predicted water levels at LTKiel (see location in Figure 2). Red line shows the mean statistical value of all 6 stations.

The model with the calibrated setting (M2) was then simulated for two independent periods and the predicted water levels were compared with the measured data (e – h in Figure 4). R^2 denotes high values in the winter months. *RMSE* slightly increases (maximum < 0.08 m) in the last two periods. As in R^2, both *SCI* and *RBI* decrease in the winter months. These results suggest that the roughness scheme of M2 can reasonably be used to simulate hydrodynamics within the RWY.

4.2.2 Nearshore hydrodynamics

Using the M2 roughness scheme (4.2.1), the nearshore hydrodynamics were simulated over the RWY, and high spatiotemporal water levels and wave heights were extracted at the monitoring stations for the EI analysis.

The predicted water levels over the RWY are shown in Figure 5 for the 6 stations with their measured data. There is a good qualitative agreement between the measured and the predicted data. Specially, the occurrence of extreme events is well captured by the model. However, the simulated water levels appear to be slightly higher than the measured data in some months (e.g., February, August in 2017). Quantitative analysis using R^2 resulted in values 0.87 - 0.90 for all locations (see Figure A3). The majority of the data points is found within the 20% limits from the line of perfect agreement.

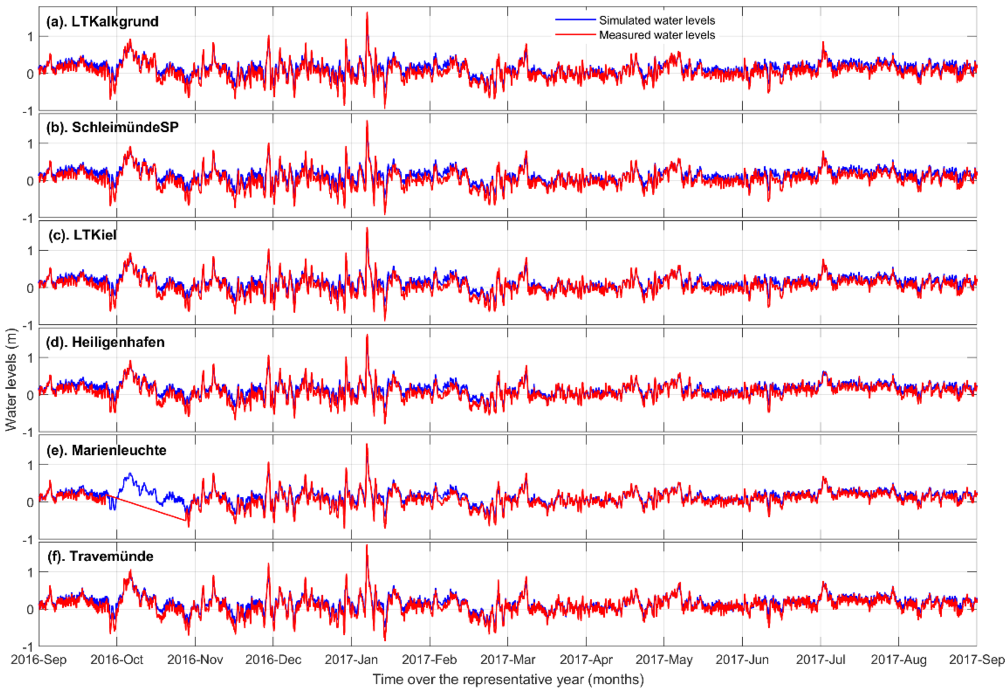

Figure 5 Comparison of measured (red) and simulated (blue) water levels at the 6 measuring stations (see Figure 2) during the RWY from 01 September 2016 to 31 August 2017: LTKalkgrund (a), SchleimündeSP (b), LTKiel (c), Heiligenhafen (d), Marienleuchte (e) and Travemünde (f).

Predicted and measured wave height comparison showed a reasonable agreement at the three buoy locations W1, W2 and W3 (Figure A4). At W1 (see location in Figure 2), the measured wave heights seem to be higher than the model prediction. It should be noted that this buoy has overestimated wave heights during the analysis period (*per. commu. with Uni. Hamburg-Harburg*). The qualitative agreement between the measured and the predicted wave heights is higher at W2 and W3 than W1. The R^2 analysis further indicates reasonable overall agreements, in which the values vary between 0.75 and 0.86 at the three buoy locations (W1: 0.84, W2: 0.75 and W3: 0.86).

4.3 Statistical analysis

This section describes the analysis of an appropriate EI for the extreme water level and wave height variations along the SH coast using the proposed 2-Step-GARMA-POT. We demonstrate the relevant steps in detail for the exemplary monitoring station 250 (Kiel Bay, see Figure 8). The implementation of the analysis was performed using the *R* packages longmemo by Maechler (2020), extRemes by Gilleland and Katz (2016) and TideHarmonics by Stephenson (2016). We exclude station 194 from the following analysis since it is a fully sheltered lagoon (Aschauhofer Lagune in Eckernförde Bay, Figure 8) resulting in constant measurements of 5 m for all time stamps.

4.3.1 Step 1

The first step fits GARMA-*k* models to all 674 (excluded 194) monitored water level and wave height series individually. When determining the number of factors *k* in the Gegenbauer models, we found that the sequential procedure of Leschinski and Sibbertsen (2019) also finds cyclic behaviour on high frequencies corresponding to periodic lengths of up to 20 minutes at the monitoring stations close to marinas. It should be mentioned that high frequencies correspond to fast moving cycles in the data. Instead of only identifying tidal constituents, we likely additionally capture contamination by ships, which pass the monitoring stations more or less regularly. For this reason, only sensible and interpretable frequencies for the GARMA-*k* model are selected, i.e., frequencies below 0.5.

Exemplary estimation results for the GARMA-*k* model fitted to the monitored time series recorded at the station 250 are reported in Table 3 (Figure A5). Since the monitoring station is located in the Kiel Bay area, the sequential procedure of Leschinski and Sibbertsen (2019) identifies a total number of 17 factors for the Gegenbauer model, of which only one frequency is below 0.5. Hence, a GARMA-1 model is fitted with ARMA orders $p = 1$ and $q = 2$ selected based on the BIC. The frequency identified as the cyclical long-range dependent component corresponds to a cycle with a natural period of $\frac{2\pi}{0.0014} \approx 28$ days corresponding to the lunar monthly tidal constituent.

Parameter	γ_1	d_1	ϕ_1	θ_1	θ_2
Value	0.0014	0.9911	0.9103	-1.7828	0.7849

Table 3 Estimation results for the GARMA-1 model fitted to the water level and wave height variations at the station 250 (see Figure 8).

A frequency coinciding with the lunar monthly tidal constituents is identified for every considered time series. For one monitoring station (station 353, see location in Figure 8), we note a lunar diurnal constituent with a period of $\frac{2\pi}{0.0436} \approx$ 23.9 h, while a total of 193 monitoring stations are found to exhibit a principal lunar semidiurnal cycle with a period of $\frac{2\pi}{0.0843} \approx$ 12.42 h. A small selection of monitoring stations appears to be subjected to additional short period cycles with periods of $\frac{2\pi}{0.1686} \approx$ 6.21 h (6 stations) and $\frac{2\pi}{0.2529} \approx$ 4.14 h (2 stations).

Figure 6 presents graphical residual diagnostics in order to assess whether all relevant cyclical long-range dependence and additional short-term correlations in the water level and wave heights time series at the station 250 are adequately captured by the fitted GARMA-1 model. The ACF of the residuals still exhibits a slight sinusoidal pattern indicating some leftover cyclicality but constitutes a large improvement over the ACF of the original series. In the periodogram of the GARMA-1 residuals, there is no longer any indication of significant peaks at any frequency. Thus, the GARMA-1 residuals resemble *iid* white noise to a reasonable extend in order to regard the assumptions of the POT model in the step 2 to be satisfied.

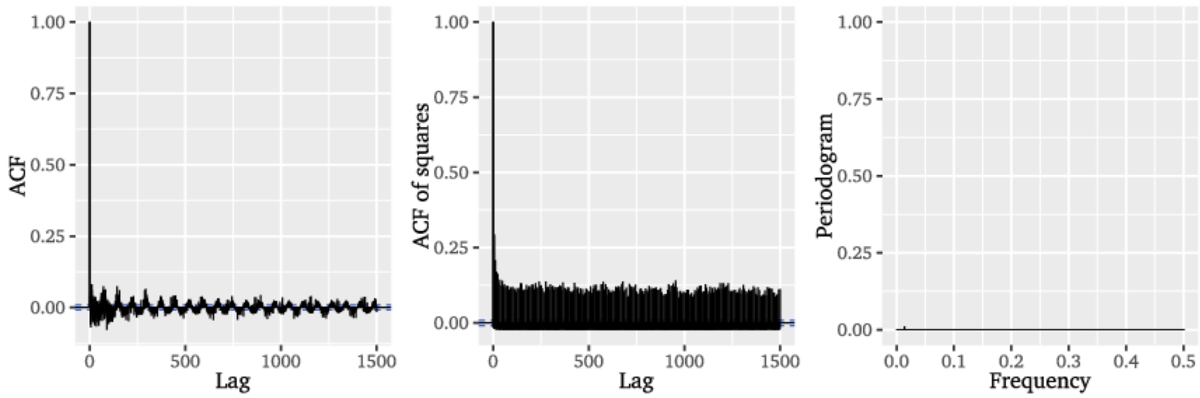

Figure 6 ACF and Periodogram of the GARMA-1 residuals for the station 250 (see location in Figure 8).

4.3.2 Step 2

In the second step, we estimate individual POT models to the residuals of the GARMA-*k* models fitted to the time series in the step 1. For that, first the automatic threshold selection procedure of Thompson et al. (2009) for each residual process is performed and then a GPD to the resulting threshold exceedances is fitted.

Parameter	***u***	**ξ**	**Σ**
Value	0.0530	-0.4583	0.0330

Table 4 Estimation results for the POT model fitted to the GARMA-1 residuals for the station 250 (see location in Figure 8). The threshold was chosen automatically using the procedure of Thompson (2009).

Exemplary, Table 4 reports the estimation results for the GARMA-1 residuals for the station 250. The automatically chosen threshold of $u = 0.053$ corresponds to a 99.49% quantile, such that 268 observations are considered extreme. Applying this quantile to the original data returns a threshold of 5.98 m. Figure 7 illustrates which GARMA-1 residuals are considered extreme based on the threshold $u = 0.053$. The threshold exceedances still exhibit a slight clustering tendency, but the QQ plot (right in Figure 7) demonstrates that the inter-event times lie within the confidence intervals of an exponential distribution (graphical diagnostics are provided in Figure A5). In the QQ plot, the GPD residuals of the GARMA-POT model lie within the confidence bands of an exponential distribution and the ACF no longer exhibits any significant autocorrelation. From these observations, we can conclude that the fitted GARMA-POT model satisfactorily characterised the seasonal long-range correlation and any additional short-range dependence.

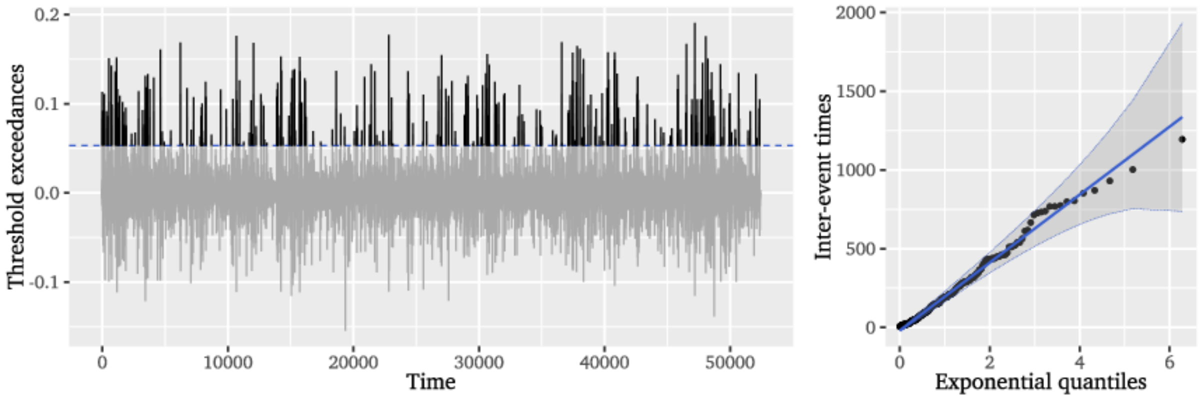

Figure 7 Exceedances for GARMA-1 residuals with automatically chosen threshold $u = 0.053$ (left) and QQ plot of the inter-event times for the station 250 (right).

The derived EI for all monitoring stations are shown in Figure 8, where the automatically chosen thresholds were translated to the corresponding quantiles in the original data and then rescaled to values in [0,1] using the min-max scaling. The smallest threshold (5.31 m) is recorded for the station 197 (Eckernförde Bay), which corresponds to an EI of 0, and the largest threshold (7.35 m) for the station 597 (east of Fehmarn, see also Figure A6-e), corresponding to an EI of 1. For clarity, zoomed-in results for the EI are provided for the regions (a) Schönhagen, (b) Stohl, (c) Schönberg, (d) Heiligenhafen, (e) Fehmarn, and (f) Dahme in Figure A6a-f.

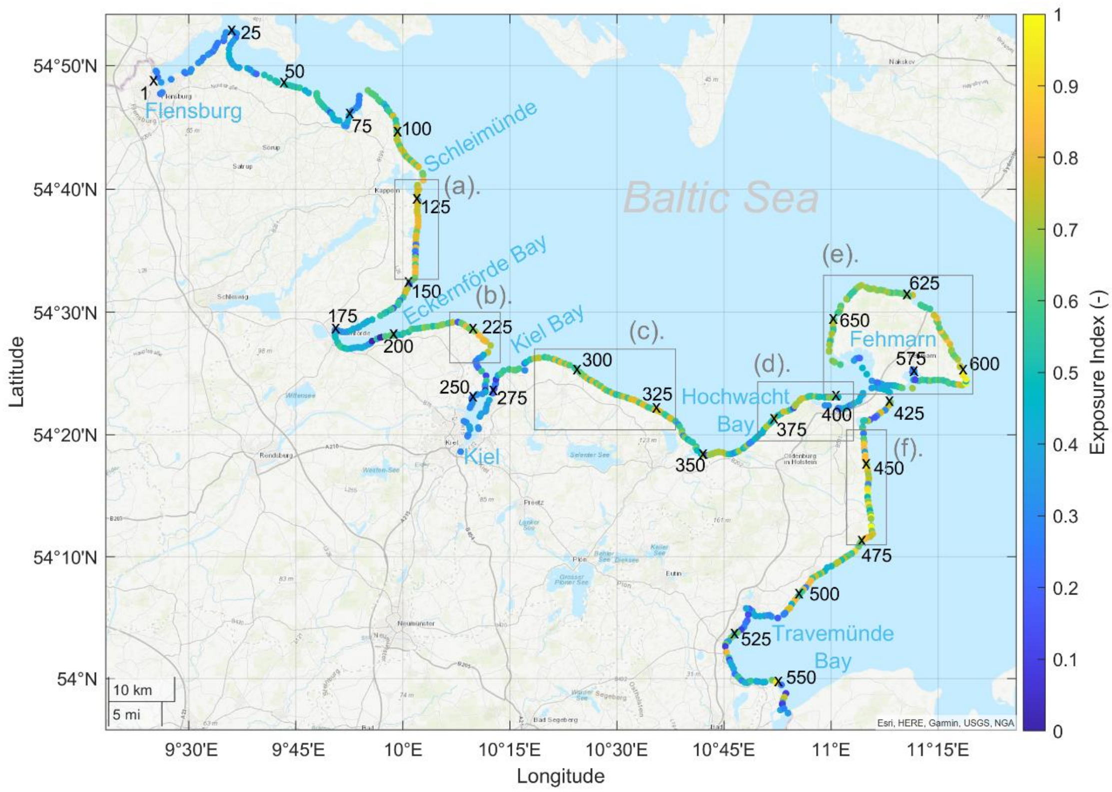

Figure 8 Derived EIs along the SH coast at the 675 monitoring stations. The colours correspond to the magnitude of the EI. A value of 0 corresponds to a threshold of 5.31 m and a value of 1 to 7.35 m (i.e., min-max scaling). The rectangles indicate the regions of (a) Schönhagen, (b) Stohl, (c) Schönberg, (d) Heiligenhafen, (e) Fehmarn, and (f) Dahme (Figure 6a-f are referred to the zoom-out views). Numbers provide the respective monitoring stations (for clarity 25-interval is marked). Source of background map: Esri, HERE, Garmin, USGS, NGA.

The EIs of all monitoring stations along the SH coast are summarised in Table A1.

5. Discussion

This study developed an Exposure Index (EI) along the Schleswig-Holstein Baltic Sea (SH) coast in Germany. The EI indicates the severity level of dynamics and hence the type of physical characteristics of the coastal system. For example, a high EI implies the occurrence of severe dynamics leading to strong erosion/sedimentation and changes at the coast and vice versa (Mason et al., 2018). Our analysis was carried out in three steps: defining a representative wind year using the measured wind data (1), numerical simulations to develop high spatiotemporal nearshore hydrodynamics (2) and statistically deriving the EI analysing model predicted nearshore water level and wave height time series (3). The EI showed high values for the coastal stretches with long fetch lengths, and low values for the areas inside bays sheltering from the wind approach.

5.1 Representative Wind Year (RWY)

For the analysis of a general value of EI, it is a pre-requisite to use representative hydrodynamic conditions along the SH coast. Such hydrodynamics can be expected during the occurrence of representative forcing to long-term data. In the semi-enclosed Baltic Sea, the hydrodynamics are governed by the occurrence of wind (LKN-SH, Bierstedt et al., 2015; Soomere, 2023). Therefore, the RWY was first defined considering the occurrence of wind in different directional sectors.

Definition of RWY was based on the measured wind data from four stations, which are distributed along the entire SH coast. These data have a high temporal resolution (10 minutes), which are sufficient to capture the major fluctuations of forcing (Lorrai et al., 2011). However, there could be errors of wind measurements at each station. Their effects on the analysis were minimized by selecting only quality-control data from DWD (https://opendata.dwd.de) and a long-term period in which short-term effects are normalised. Span of the data set at each station covers different periods. Therefore, a common period of 20 years from 2000 to 2019 was hereon selected for the analysis. The dominant wind directions at the stations are from the SW to NW sector (see Figure A1), while strong wind still occurred from the NE to SE sector albeit with low probability. The local wind characteristics depend on the orientation of the coastline. At Schönhagen, wind approached over the land in the dominant sector, while it is over water at the other three stations. Therefore, the wind characteristics of Schönhagen might be performed differently in the analysis compared to the other locations (see Figure 3).

A wind year was classified from summer to summer of the adjacent years. The aims of this classification were twofold in contrast to the selection of a calendar year. First is to avoid the separation of winter storm events that occurred at the end of December. Second, an occurrence of strong and persistence winds in the winter months can be expected. Although individual storm events can be separately identified from December to January, they might be related to a same meteorological event: storm cluster (e.g., Dissanayake et al., 2015). Our classification further complies with the wind statistics at the measuring stations, of which the month of the lowest wind in each year from 2000 to 2019 is generally found in the period from August – September (DWD).

The RWY was analysed considering the occurrence of wind speeds in different directional sectors. For the analysis, we used wind speed as the main parameter because the higher the wind speed the stronger the sea state leading to high dynamics (Bierstedt et al., 2015). In other words, high wind speeds with short fetch could results in strong sea state than the case of low wind speed and long fetch (e.g., Hs = 2.1 m for wind speed 40 kt and fetch 20 km, and Hs = 1.2 m for wind speed 20 kt and fetch 40 km for cases of constant wind direction lasting for 5 hours). Furthermore, for the same wind speed, the strength of dynamics at the coast might vary depending on the existing fetch length (Soomere, 2023; Mason et al., 2018). Therefore, we analysed the wind data with 5 m/s speed intervals (6 classes from 0 – 30 m/s) and in 10^o sectors (36 from 0^o to 360^o), which might be sufficient to capture the existing fetch lengths at any point along the coast. The comparison between overall wind climate and each wind year was performed in terms of the occurrence of wind speed in each directional sector, which provides a good basis to capture the availability of different fetch lengths depending on the coastline orientations at the set locations along the SH coast.

The RWY was defined considering the performance of statistical values at the 4 stations together (Figure 3). For all statistical parameters, Schönhagen showed different variations along the wind years than the other three stations. This could be due to the fact, that wind approaches over the land at Schönhagen in contrast to the others as explained above. The best value of an individual location might not necessarily be captured while considering all stations together. For example, the lowest *rmsd* and the highest *Skill* at Warnemünde are 0.32 m/s and 0.93 respectively for the wind year 01 September 2003 – 31 August 2004, while they are 0.32 m/s and 0.94 at Darss for the wind year 01 September 2012 – 31 August 2013. As the 4 stations are distributed along the entire coast of the model domain (see SH grid in Figure 1), it is required to identify a value satisfying all stations. Then, a more realistic wind forcing on the hydrodynamic computation can be expected. The selected RWY (01 September 2016 – 31 August 2017) has the optimal statistical values (e.g., *rmsd*: 0.56 m/s and *Skill*: 0.77), and that is further convinced by comparing the wind roses, i.e., occurrence of wind speeds and directions (see Figure A1).

5.2 Nearshore hydrodynamics

The Baltic Sea coast in general and the SH coast in particular has a narrow surf zone. For example, in front of the Stohl coast, strong hydrodynamics are limited to a cross-shore stretch of about 500 m extending up to about 5 m depth, and the alongshore littoral drift dominates within the first 200 m therein (Dissanayake and Winter, 2023). These characteristics can be expected along the entire SH coast based on the existence of a shallow nearshore area (see Figure 2). Therefore, we selected 5 m depth to monitor the variations of water levels and wave heights, which can be used to represent the severity of nearshore hydrodynamics (Dissanayake et al., 2021a), by simulating a model nesting of two domains. Of which, the fine-domain (SHC) has the highest cross-shore resolution of 75 m. Our sensitivity analyses showed that such resolution is sufficient to monitor hydrodynamics around 5 m water depth, whereas a grid setup of higher resolution than SHC is highly recommended to predict hydrodynamics closer to the beach (e.g., Dissanayake and Winter, 2023). On the other hand, it is not feasible to use a very fine grid setup covering the SH coast of about 400 km in length. Therefore, the SHC model provides sufficiently accurate hydrodynamic parameters for our analysis.

Analysis of an EI based on geometrical fetch lengths might not provide accurate values for a complex coastal system. In early studies, exposure was derived based on solely the geometrical fetch (e.g., Mason et al., 2018; Keddy, 1982). Depending on the existing nearshore morphological features and coastline orientations, there could be a significant difference of fetch lengths of adjacent points along a coast. However, when high water levels and currents occur at a location due to exposing to long fetch, these hydrodynamics certainly affect to the adjacent locations irrespective to their prevailing fetch lengths. This phenomenon cannot be taken into account while analysing exposure based on the geometrical fetches. The SH coast is a complex system, which consists of different morphological features and coastline orientations (Averes et al., 2021). Therefore, the analysis using nearshore hydrodynamics is very appropriate to develop more accurate EI values indicating the state of the coast.

Predicted hydrodynamics could incur some limitations due to a number of reasons. Based on the applied grid resolution (i.e., 75 m), the model bathymetry might not capture nearshore topography accurately. As mentioned earlier, the objective of the present approach is to define a general EI along the SH coast and to identify the erosion hotspots. At the identified coastal stretches, it is required to repeat this analysis to develop accurate hydrodynamics applying high resolution (~ 2 m) local models. Furthermore, there could be errors in the bathymetry data from BSH and IOW, which are unavoidable. For the model forcing, water levels were used from the large-scale model of Gräwe et al. (2015), which does not predict a 1:1 agreement with the measured water levels. Spatiotemporal wind fields from COSMO are reanalysis data, and they have magnitude and phase agreements > 0.9 and <-10^o respectively compared with the measured wind data (Figure A2). Moreover, assumptions and approximations of the numerical model itself can cause limitations of the predicted hydrodynamics. With all these potential complications, our approach in predicting nearshore hydrodynamics provided however reasonable overall agreements with the measured data (R^2: 0.87-0.90 for water levels and 0.75-0.86 for wave heights) enabling a reliable basis for the analysis of an accurate EI along the SH coast.

5.3 Exposure Index (EI)

Our approach allows the extension of the POT method to dependent as well as cyclical data (Dissanayake et al., 2021a,b). Usually the POT methodology is constructed for independent data as any type of dependence leads to strong clustering of extremes, and so does also cyclical behaviour of the data. A priori estimating and filtering possible cycles and dependencies in the data allow the application of the standard POT method to identify independent residuals. This allows finding thresholds in the residuals, which define quantiles of extremes, which can then again be used to derive a valid threshold for the original data avoiding the clustering of extremes (Scarrott and MacDonald, 2012).

Applying a priori estimation and filtering step might introduce an estimation error, which in our situation may especially problematic, if the cyclical frequency is not estimated correctly. However, Leschinski and Sibbertsen (2019) prove consistency of their method with the fastest possible rate of convergence. Given the large amount of data available for the Baltic Sea the estimation error is negligible in our situation.

The estimated EIs have high spatial resolution (i.e., 500 m apart) and show considerable variability along the SH coast. There are low values in the bays and in the sheltered areas along the coast, while high values are found along the exposed coastal stretches (see Figure 8, Figure A6a-f and Table A1) indicating potential hotspots of erosion, which demand more management intervention. However, it should be emphasized that there are no high values along the entire exposed stretches as we set our hypothesis, in contrast to an analysis using fetch lengths (Mason et al., 2018). Present analysis is based on the predicted water levels and wave heights (~5 m depth) along the coast, which are driven by wind being the main driver of hydrodynamics (Soomere, 2023), and vary depending on the nearshore morphological features of this complex coast (Averes et al., 2021). Moreover, local water levels and wave heights drive therein current pattern, and thus sediment transport and morphodynamics determining the state of the coast (Dissanayake et al., 2022). On the other hand, a definition of the EI based on fetch lengths (e.g., Mason et al., 2018) does not necessarily capture the status of local coasts. In contrast, the present novel definition using high spatiotemporal nearshore hydrodynamics indicates high resolution spatial characteristics of local coasts, and therefore could be highly variable along a coast even with a long fetch. This approach can be further improved by repeating the analysis at the identified erosion hotspots using high spatial resolution model domains, in which the nearshore morphology is well represented, and so does the nearshore hydrodynamics (e.g., Dissanayake and Winter, 2023). Furthermore, the developed 3-step method (RWY, prediction of hydrodynamics and definition of EI) can be easily transferable for any coastal system, and to investigate the alongshore variability of the general coastal state.

6. Conclusions

The Schleswig-Holstein Baltic Sea (SH) coast is a complex coastal system consisting of different morphological features and coastline orientations enabling different exposures to winds and waves. Though the dominant wind approach is from SW to NW, extreme events occur from N to E being exposed to long fetches causing strong local dynamics, which vary depending on the nearshore morphology. Therefore, an exposure index (EI), which is derived based on the local hydrodynamics, can be used as a proxy to demonstrate the susceptibility of this coast to marine forcing (e.g., identifying potential erosion hotspots). We employed a 3-step approach to define high resolution (500 m apart along the entire SH coast of ~400 km) and more accurate EIs: defining a representative wind year (RWY), predicting high spatiotemporal nearshore (~5 m depth) hydrodynamics by numerical modelling and statistically deriving EI using predicted water levels and wave heights over RWY.

To investigate under the general characteristics of forcing, it is a pre-requisite to contemplate a representative period to long-term data. In the Baltic Sea, wind is the main driver of marine forcing. Therefore, the RWY was defined by analysing the measured wind data from 2000 to 2019 at 4 stations, which are distributed along the entire area of interest. This analysis focused on the occurrence of wind speeds in 36 directional sectors, as the wind speed is important for the sea state rather than fetch for the given direction. Based on the long-term wind statistics at the measuring stations, a wind year was defined from summer to summer of adjacent years, which accommodates winter storms in a single year. The identified RWY (01.09.2016 – 31.08.2017) showed a good resemble to the entire wind climate of 20 years (e.g., *rmsd*: 0.56 m/s and *Skill*: 0.77). High spatiotemporal hydrodynamics for the SH coast were predicted using a model nesting of 2 domains (highest resolution ~75 m) in Delft3D. The model setup was initially calibrated, and validated for two independent periods tuning the bed roughness schemes. Predicted nearshore hydrodynamics over the RWY provided reasonable agreements with the measured data (R^2: 0.87 – 0.90 for water levels and 0.75 – 0.86 for wave heights). In a two-step procedure, we developed EIs based on a generalization of the classical POT model for cyclical and dependent data. Estimating and filtering the cycles and dependencies allow to apply the standard POT methods to the residuals and to identify thresholds, first for the residuals and then for the original data, which avoid strong clustering of extremes.

The exposed areas display high EIs (e.g., 1 at the east of Fehmarn, Figure A6-e), while sheltered areas have low values (e.g., 0 at Eckernförde Bay, Figure 8). The expose of the coast to strong dynamics are therefore manifested by EIs, which can be used to identify the potential erosion hotspots requiring more management interventions. In contrast to the previous definitions using fetch lengths, our approach showed high variability of the EI even for the exposed coastal stretches. Local hydrodynamics depend on the nearshore morphology, and thus variable EI though exposing to long fetches. Therefore, the present definition of EI provides a more accurate interpretation of the susceptibility of a coast to marine forcing. The credibility of this approach certainly increases by comparing the EIs with long-term morphological changes along the SH coast, and repeating the analysis at the identified erosion hotspots using high spatial resolution model domains. The developed 3-step method can be easily transferable for any coastal system to define an EI, and to investigate the alongshore variability of the coastal status, which might indicate the vulnerable coastal stretches.

Data availability statement

This study used different open source data and modelling tools, which are referred to the respective sources in the text: Bathymetry data from Federal Maritime and Hydrography Agency (BSH) (https://www.geoseaportal.de) and Baltic Sea Research Warnemünde (IOW) (https://www.io-warnemuende.de/topography-of-the-baltic-sea.html), coastline from European Environmental Agency (EEA) (https://www.eea.europa.eu),Wind data from the German Weather Service (DWD) (https://opendata.dwd.de), and the Delft3D modelling tool from Deltares (delft3d - Revision 142633: / (deltares.nl)).

Acknowledgement

This study was carried out as a part of the project MorphoPro (Morphological Projections for the Schleswig-Holstein Baltics Sea coast in 2100) funded by the Federal State Government Schleswig-Holstein. Results shown on this paper are based on the numerical simulations carried out on the CAU (Kiel University) NEC-HPC cluster. PD acknowledges the Local Agency for Coastal Protection (LKN.SH) for providing necessary data, the colleagues from the institute of River and Coastal Engineering (University of Hamburg-Harburg) for working together in this project, and Christian Winter (CAU) for the initial guidance of this study. PD greatly acknowledges Coastal Research Station of the Federal State Government Lower Saxony (NLWKN) and the ongoing EU project REST-COAST (www.rest-coast.eu) during which the last part of this study was conducted.

References

Balkema, A. A. and de Haan, L., 1974. Residual life time at great age, The Annals of Probability 2.5.

Bernardara, P., Andreewsky, M., Benoit, M., 2011. Application of regional frequency analysis to the estimation of extreme storm surges, Journal of Geophysical Research 116.C2.

Bierstedt, S., Hünicke, B., Zorita, E., 2015. Variability of wind direction statistics of mean and extreme wind events over the Baltic Sea region, Tellus A, 67, 29073.

Booij, N., Ris, R.C., Holthuijsen, L.H., 1999. A third-generation wave model for coastal regions, Part I, Model description and validation. J. Geophys. Res., 104, 7649–7666.

Brüning, T., Janssen, F., Kleine, E., Komo, H., Maßmann, S., Menzenhauer-Schmacher, I., Jandt, S., Dick, S., 2018. Operationelle Ozeanvorhersage für deutsche Küstengewässer, Die Küste 86, 293-310.

Burton, T. M., Uzarski, D. G., Genet, J. A., 2004. Invertebrate habitat use in relation to fetch and plant zonation in northern Lake Huron coastal wetlands. Aquatic Ecosystem Health & Management 7(2), 249–267, https://doi.org/10.1080/14634980490461614.

Cañellas, B., Orfila, A., Méndez, F.J., Menéndez, M., Gómez-Pujol., L., Tintoré, J., 2007. Application of a POT model to estimate the extreme significant wave height levels around the Balearic Sea (Western Mediterranean), Journal of Coastal Research, 329–333.

Coles, S., 2009. An introduction to statistical modeling of extreme values. 3. print., Springer series in statistics. Springer: London, United Kingdom.

Davison, A.C., Smith, R.L., 1990. Models for exceedances over high thresholds, Journal of the Royal Statistical Society: Series B (Methodological) 52.3, 393–425.

Dissanayake, P., Brown, J., Sibbertsen, P., Winter, C., 2021a. Using a two-step framework for the investigation of storm impacted beach/dune erosion, Coastal Engineering 168, 103939.

Dissanayake, P., Brown, J., Wisse, P., Karunarathna, H., 2015. Comparison of storm cluster vs isolated event impacts on beach/dune morphodynamics, Estuarine, Coastal and Shelf Science 164, 301-312.

Dissanayake, P., Flock, T., Meier, J., Sibbertsen, P., 2021b. Modelling Short- and Long-term Dependencies of Clustered High-Threshold exceedences in significant wave heights, Mathematics 9, 2817.

Dissanayake, P., Winter, C., Averes, T., Krämer, K., Sone, H., Dreier, N., Nehlsen, E., Fröhle, P., Hirschhäuser, T., 2022. Effect of large-scale forcing on the local sediment transport potential at the Schleswig-Holstein Baltic Sea coast, Pro. International Conference of Coastal Engineering (ICCE), Sydney, Australia.

Dissanayake, P., Winter, C., 2020. Modelling the coastline orientation on storm erosion at the Sylt island, North Sea. In Proceedings of the virtual Conference of Coastal Engineering, 36v, paper 20.

Dissanayake, P., Winter, C., 2023. Modelling morphodynamic potential at local scale along the Scheleswig-Holstein Baltic Sea coast, Pro. Coastal Sediment conference, New Orleans, USA.

Dreimanis, A., Lundqvist, J., 1984. What should be called till? Striae, 20, 5–10.

Ehlers, J., 2020. Das Eiszeitalter; Springer: Berlin, Heidelberg, Germany.

Embrechts, P., Klüppelberg, C., Mikosch, T., 2012. Modelling extremal events for insurance and finance: For Insurance and Finance. Vol. 33, Applications of mathematics. Berlin: Springer.

Fleming, K., Johnston, P., Zwartz, D., Yokoyama, Y., Lambeck, K., Chappell, J., 1998. Refining the Eustatic Sea-Level Curve since the Last Glacial Maximum Using Far- and Intermediate-Field Sites. Earth Planet. Sci. Lett., 163, 327–342.

Gilleland, E., Katz, R.W., 2016. extRemes 2.0: An extreme value analysis package in R, Journal of Statistical Software 72.8.

Giraitis, L., Leipus, R., 1995. A generalized fractionally differencing approach in long-memory modelling, Lithuanian Mathematical Journal 35.1, 53–65.

Gray, H. L., Zhang, N.-F., Woodward, W. A., 1989. On generalized fractional processes, Journal of Time Series Analysis 10.3, 233–257.

Gräwe. U., Burchard, H., 2012. Storm surges in the western Baltic Sea: the present and a possible future, Climate Dynamics 39, 165-183.

Gräwe, U., Naumann, M., Mohrholz, V., Burchard, H., 2015. Anatomizing one of the largest saltwater inflows into the Baltic Sea in December 2014, Journal of Geophysical Research: Oceans 120, 7676-7697.

Hunt, S., Bryan, K.R., Mullarney, J.C., 2017. The effect of wind waves on spring-neap variations in sediment transport in two meso-tidal estuarine basins with contrasting fetch. Geomorphology, 280, 76–88.

Håkanson, L. A., 1981. Manual of Lake Morphometry (Berlin: Springer-Verlag).

Kalff, J., 2002. Limnology: inland water ecosystems (Upper Saddle River, N.J).

Keddy, P. A., 1982. Quantifying within-lake gradients of wave energy: interrelationships of wave energy, substrate particle size and shoreline plants in Axe Lake, Ontario. Aquatic Botany 14, 41–58.

Landesbetrieb Für Küstenschutz, Nationalpark Und Meeresschutz Des Landes Schleswig-Holstein (LKN-SH). Fachplan Küstenschutz Ostseeküste. Grundlagen. Available online: schleswig-holstein.de - Küstenschutz Fachpläne - Fachplan Küstenschutz Ostseeküste

Leadbetter, M. R., 1991. On a basis for 'Peaks over Threshold' modeling, Statistics & Probability Letters 12.4, 357–362

Leschinski, C., Sibbertsen, P., 2019. Model order selection in periodic long memory models, Econometrics and Statistics 9, 78–94.

Lesser, G., Roelvink, J.A., Van Kester, J.A.T.M., Stelling, G.S., 2004. Development and validation of a three-dimensional morphological model. Coastal Engineering, 51, 883–915.

Lorrai, C., Umlauf, L., Becherer, J.K., Lorke, A., Wüest, A., 2011. Boundary mixing in lakes: 2. Combined effects of shear and convectively induced turbulence on basin-scale mixing. J Geophys Res. 116(C10018):1–12.

Maechler, M., 2020. longmemo: Statistics for long-memory processes (Book Jan Beran), and related functionality.

Mann, K. H., Lazier, J. R., 2013. Dynamics of marine ecosystems: biological-physical interactions in the oceans. (John Wiley & Sons, 2013).

Marsh, W. M., Marsh, B. D., 1987. Wind erosion and sand dune formation on high Lake Superior bluffs. Geogr. Ann 69A, 379–391.

Mason, L.A., Riseng, C.M., Layman, A.J., Jensen, R., 2018. Effective fectch and relative exposure index maps for the Laurentian Great Lakes, Scientific Data, 5:180295, doi: 10.1038/sdata.2018.295.

Metzner, M., Gade, M., Hennings, I., Rabinovich, A., 2000. The observation of seiches in the Baltic Sea using a multi data set of water levels, Journal of Marine Systems, 24, 1-2, 67-84.

Minns, C. K., Wichert, G. A., 2005. A framework for defining fish habitat domains in Lake Ontario and its drainage. J. Great Lakes Res. 31, 6–27.

Méndez, F.J., Menéndez, M., Luceño, A., Losada, I.J., 2006. Estimation of the long-term variability of extreme significant wave height using a time-dependent Peak Over Threshold (POT) model, Journal of Geophysical Research 111.C7.

Pickands III, J., 1975. Statistical inference using extreme order statistics, The Annals of Statistics 3.1.

Plattner, S., Mason, D. M., Leshkevich, G. A., Schwab, D. J., Rutherford, E. S., 2006. Classifying and forecasting coastal upwellings in Lake Michigan using satellite derived temperature images and buoy data. J. Great Lakes Res. 32, 63–76)

Randall, R. G., Minns, C. K., Cairns, V. W., Moore, J. E., 1996. The relationship between an index of fish production and submerged macrophytes and other habitat features at three littoral areas in the Great Lakes. Can. J. Aquat. Sci. 53, 35–44.

Scarrott, C., MacDonald, A., 2012. Review of extreme value threshold estimation and uncertainty quantification, REVSTAT-Statistical Journal 10.1, 33–60.

Schwab, D. J., Beletsky, D., Lou, J., 2000. The 1998 coastal turbidity plume in Lake Michigan. Estuarine, Coastal and Shelf Science 50, 49–58.

Soomere, T., 2023. Numerical simulations of wave climate in the Baltic Sea: a review, Earth System Changes in Marginal Seas/Oceanologia 65, 117-140.

Stelling, G.S., 1984. On the construction of computational methods for shallow water flow problem. In Rijkswaterstaat Communications; Governing Printing Office: Hague, The Netherlands, Volume 35.

Stelling, G.S., Lendertse, J.J., 1991. Approximation of Convective Processes by Cyclic ACI methods. In Proceedings of the 2nd ASCE Conference on Estuarine and Coastal Modelling, Tampa, FL, USA, 13–15 November.

Stephenson, A., 2016. Harmonic analysis of tides using TideHarmonics.

Thompson, P., Cai, Y., Reeve, D., Stander, J., 2009. Automated threshold selection methods for extreme wave analysis, Coastal Engineering 56.10, 1013–1021.

Uzarski, D. G., Burton, T. M., Genet, J.A., 2004. Validation and performance of an invertebrate index of biotic integrity for Lake Huron and Michigan fringing wetlands during a period of lake level decline. Aquat. Ecosyst. Health 7, 269–288.

Van Ormondt, M., Nelson, T.R., Hapke, C.J., Roelvink, D., 2020. Morphodynamic modelling of the wilderness breach, Fire Island, New York. Part I: Model set-up and validation. Coast. Eng., 157, 103621.

Woodward, W. A., Cheng, Q. C., Gray, H. L., 1998. A k-factor GARMA long-memory model, Journal of Time Series Analysis 19.4, 485–504.

Yurista, P. M., Kelly, J. R., Scharold, J.V., 2016. Great Lakes nearshore–offshore: Distinct water quality regions. J. Great Lakes Res. 42, 375–385.

Ziegler, B., Heyen, A., 2005. Rückgang der Steilufer an der schleswig-holsteinischen westlichen Ostseeküste. Meyniana, 57, 61–92

Annex

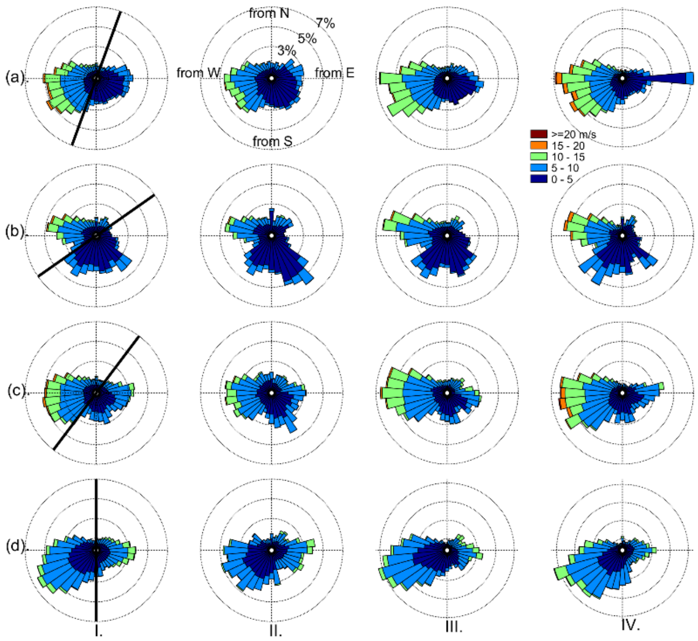

Figure A1: Comparison of wind roses from measured data (Column I, a. Schönhagen, b. Fehmarn, c. Warnemünde and d. Darss) and defined wind years, Weak (Column II), Representative (Column III) and Strong (Column IV). Black line indicates the orientation of the coastline at the measuring station.

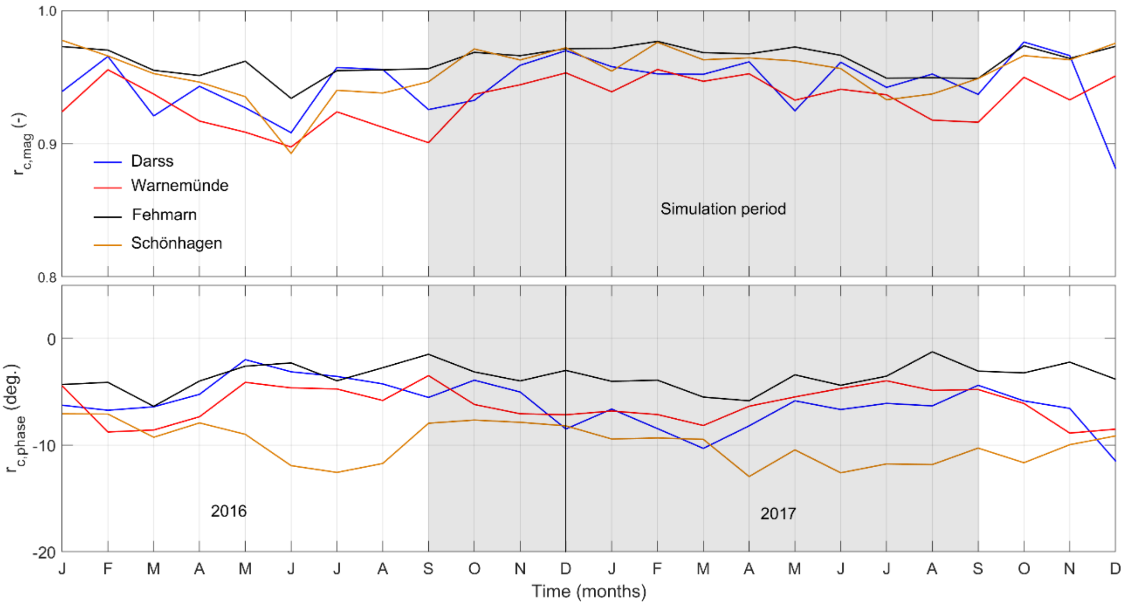

Figure A2: Statistical comparison between measured wind data at 4 stations and those from spatial analysed COSMO wind data from DWD (https://opendata.dwd.de) showing the variation during the representative year, 01 September 2016 to 31 August 2017.

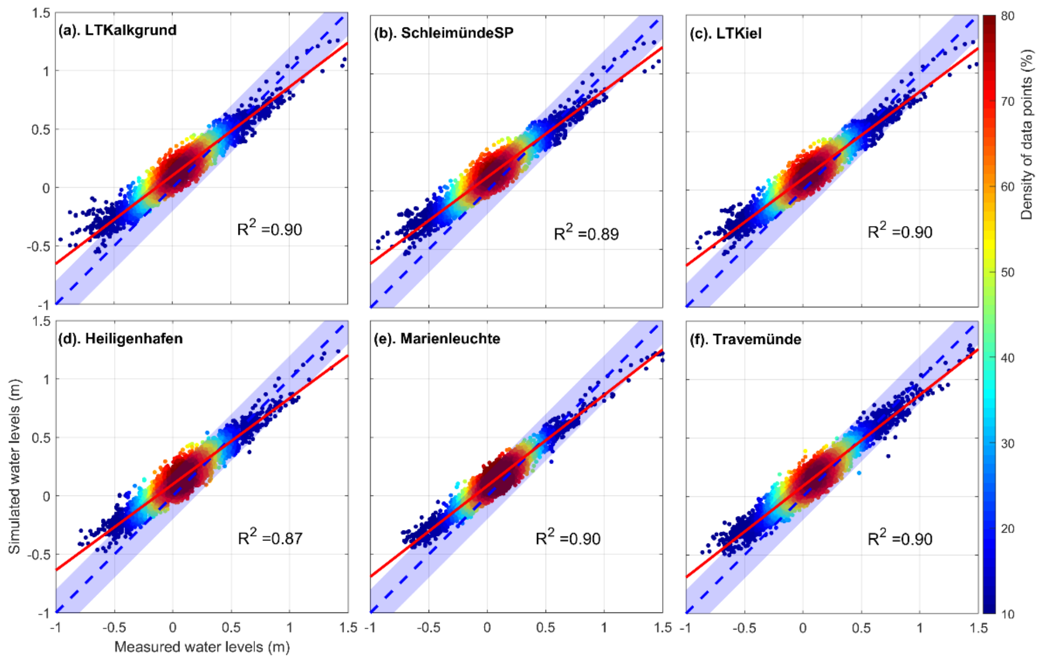

Figure A3: Comparison of measured and simulated water levels at 6 stations (see Figure 2). Red line indicates the best fit and the density of data points is shown by colours. Blue shadow area shows the 20% of deviation from the perfect agreement between measured and predicted water levels.

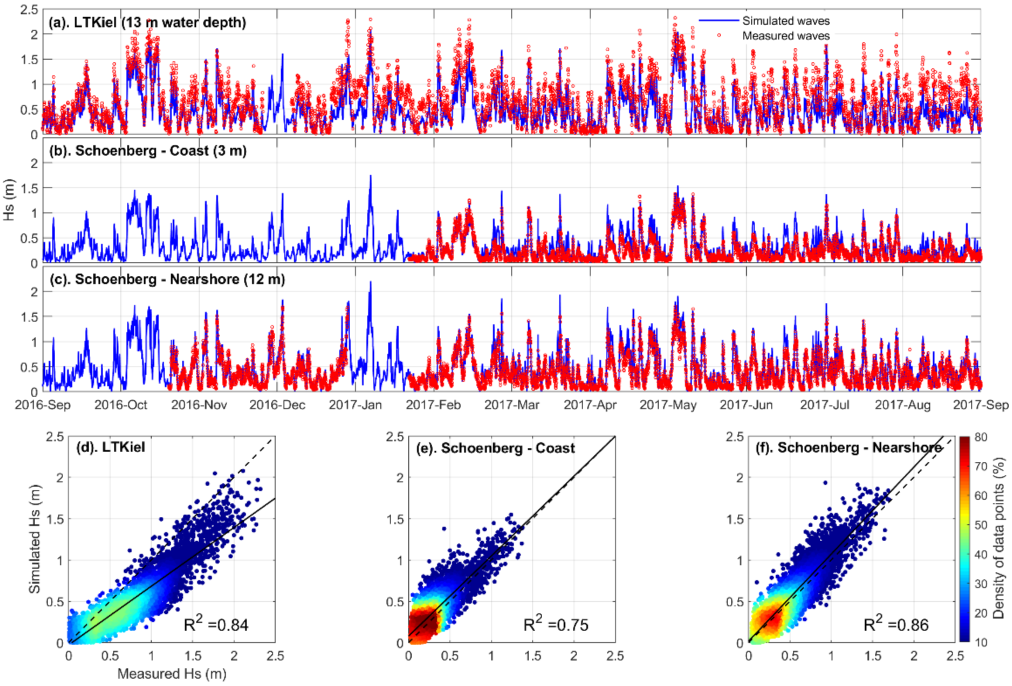

Figure A4: Comparison of measured and simulated wave heights at 3 stations (see locations in Figure 2). (a) – (c): qualitative comparison, and (d) – (f): statistical comparison. Dash line indicates perfect agreement, and solid line shows the best fit between measured and predicted wave heights. Colour show the density of data points.

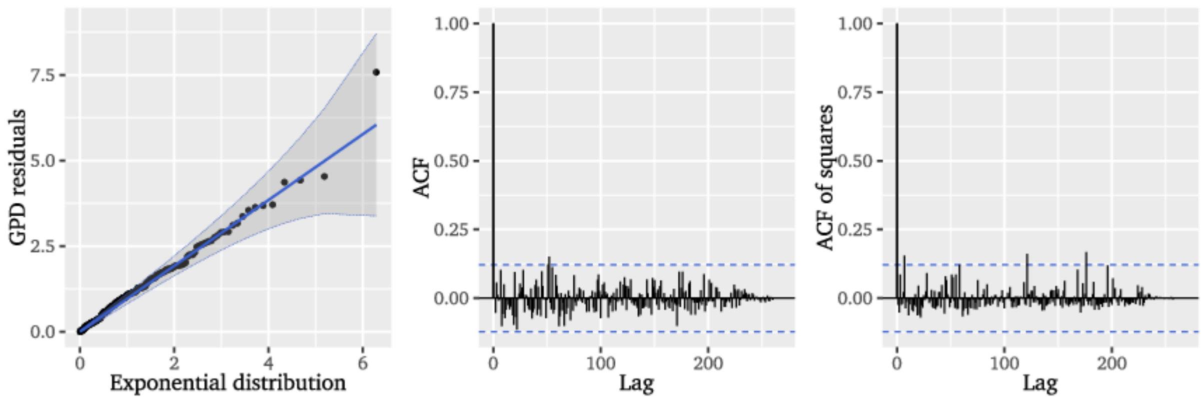

Figure A5: Unit exponential QQ-plot (left) and ACF of GPD residuals (middle and right) of the GARMA-POT for the station 250 (see Figure 8).

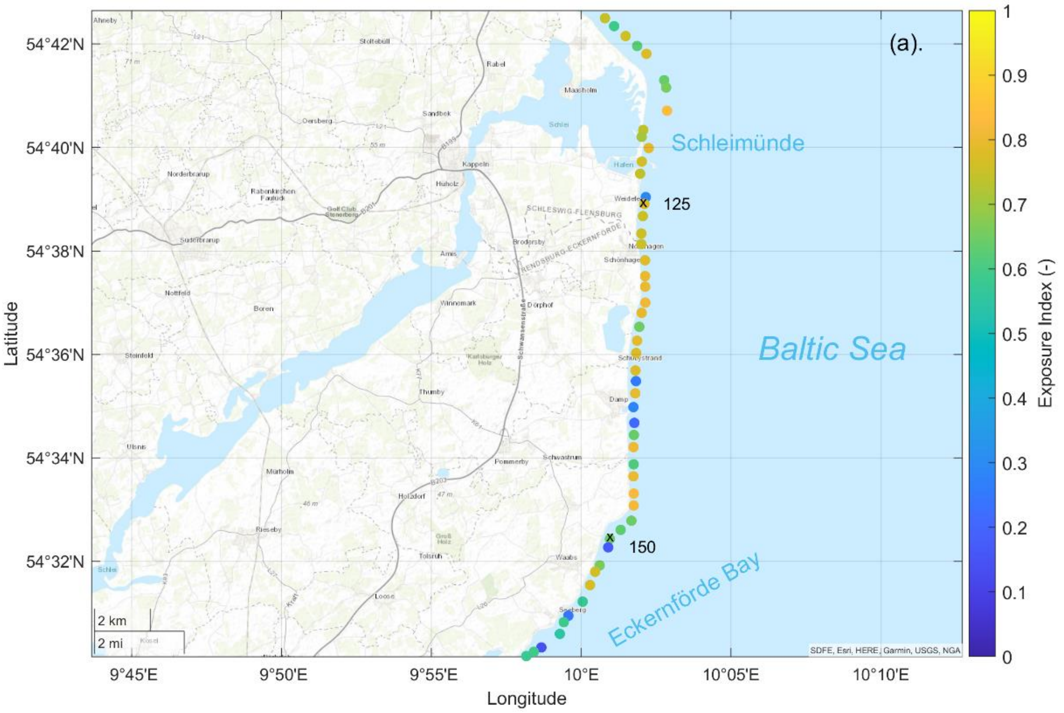

Figure A6-a Estimated EI within the selected zoom-out window: Schönhagen (see (a) in Figure 8). The colours correspond to the value of the EI at the specific monitoring station. A value of 0 corresponds to a threshold of 5.31 m and a value of 1 to 7.35 m (i.e., min-max scaling). Source of background map: SDFE, Esri, HERE, Garmin, USGS, NGA.

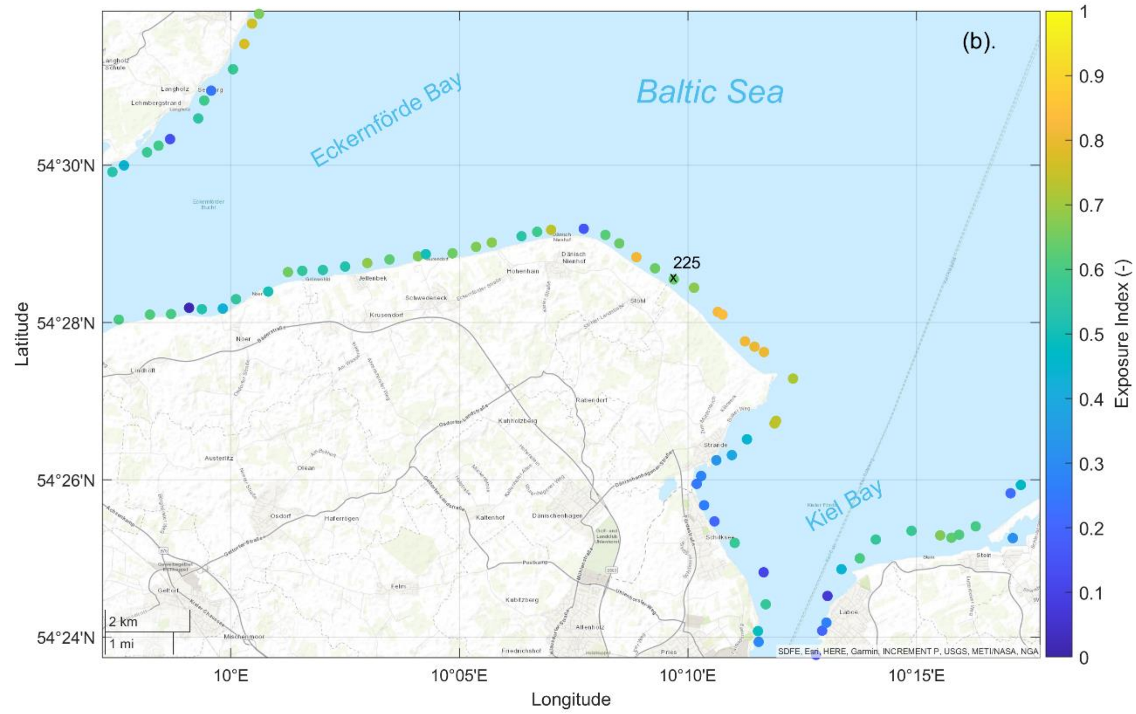

Figure A6-b Estimated EI within the selected zoom-out window: Stohl (see (b) in Figure 8). The colours correspond to the value of the EI at the specific monitoring station. A value of 0 corresponds to a threshold of 5.31 m and a value of 1 to 7.35 m (i.e., min-max scaling). Source of background map: SDFE, Esri, HERE, Garmin, INCREMENT P, USGS, METINASA, NGA.

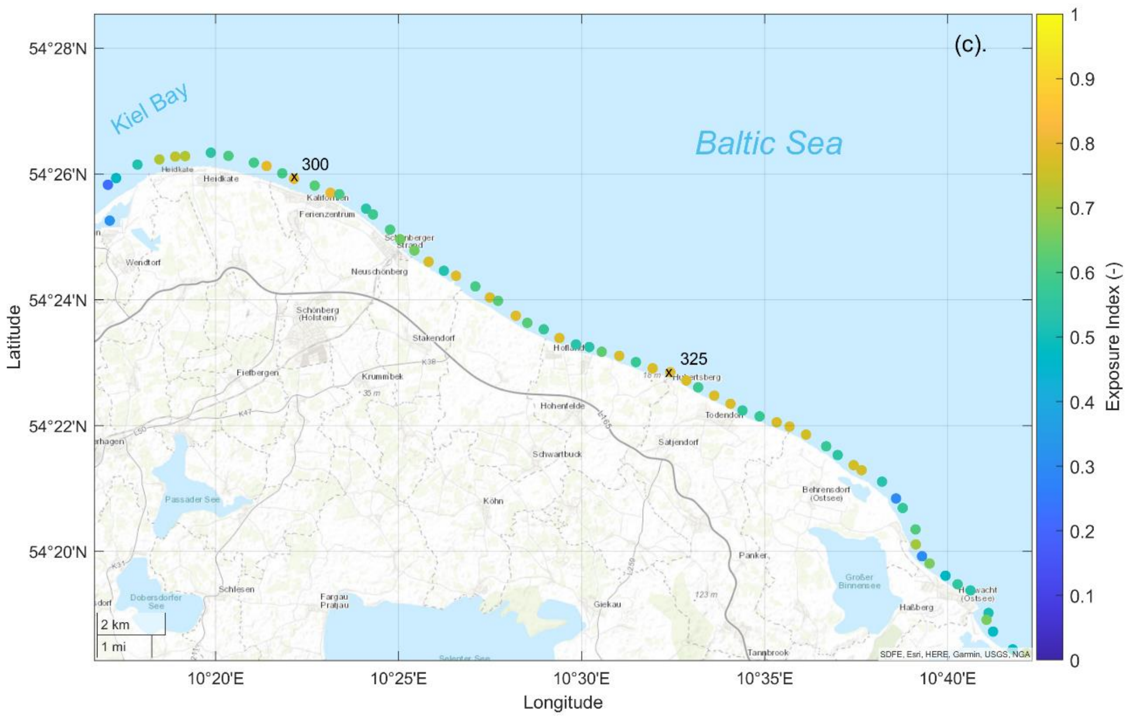

Figure A6-c Estimated EI within the selected zoom-out window: Schönberg (see (c) in Figure 8). The colours correspond to the value of the EI at the specific monitoring station. A value of 0 corresponds to a threshold of 5.31 m and a value of 1 to 7.35 m (i.e., min-max scaling). Source of background map: SDFE, Esri, HERE, Garmin, USGS, NGA.

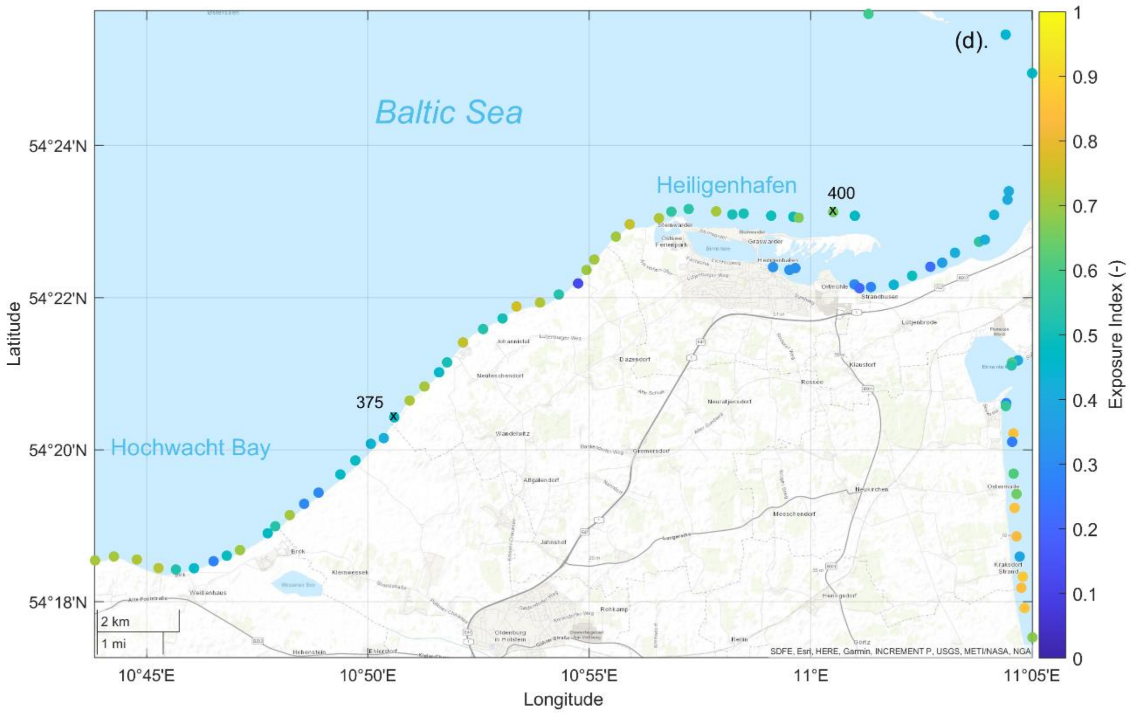

Figure A6-d Estimated EI within the selected zoom-out window: Heiligenhafen (see (d) in Figure 8). The colours correspond to the value of the EI at the specific monitoring station. A value of 0 corresponds to a threshold of 5.31 m and a value of 1 to 7.35 m (i.e., min-max scaling). Source of background map: SDFE, Esri, HERE, Garmin, INCREMENT P, USGS, METINASA, NGA.

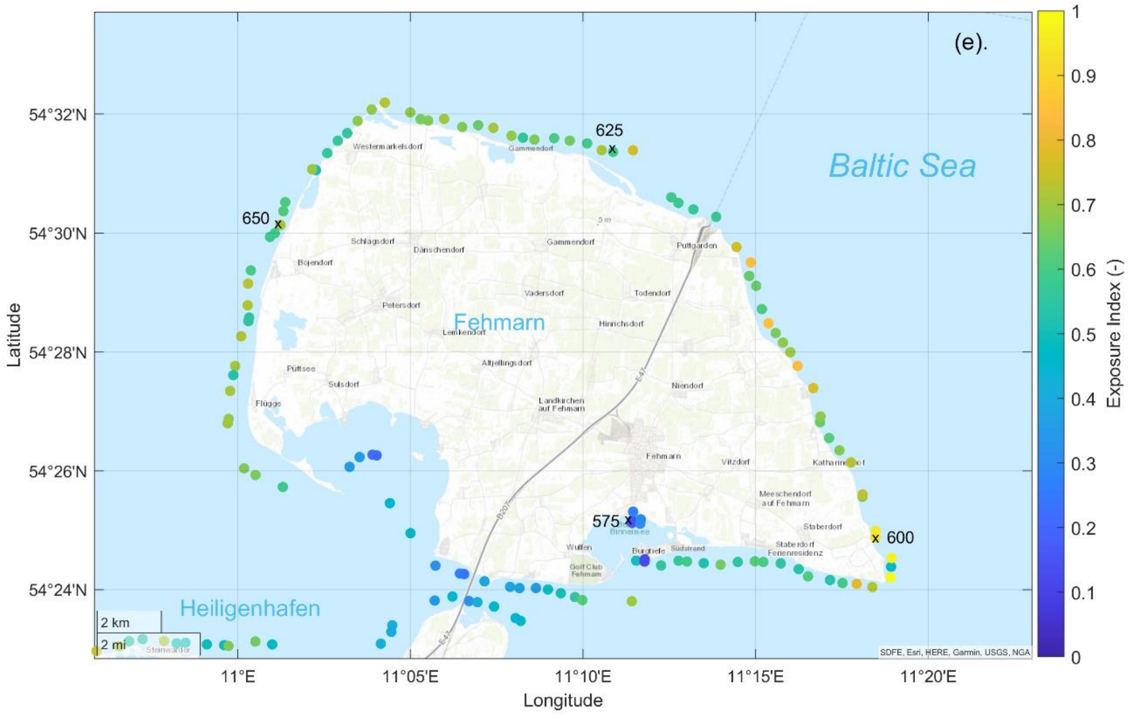

Figure A6-e Estimated EI within the selected zoom-out window: Fehmarn (see (e) in Figure 8). The colours correspond to the value of the EI at the specific monitoring station. A value of 0 corresponds to a threshold of 5.31 m and a value of 1 to 7.35 m (i.e., min-max scaling). Source of background map: SDFE, Esri, HERE, Garmin, USGS, NGA.

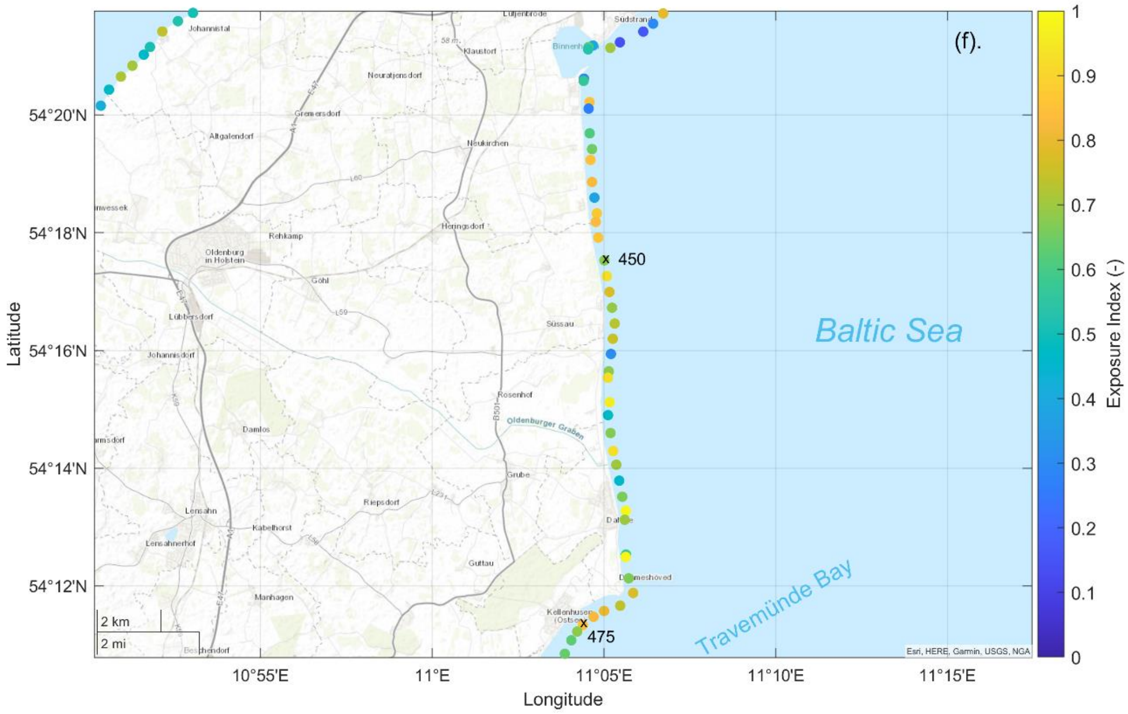

Figure A6-f Estimated EI within the selected zoom-out window: Dahme (see (f) in Figure 8). The colours correspond to the value of the EI at the specific monitoring station. A value of 0 corresponds to a threshold of 5.31 m and a value of 1 to 7.35 m (i.e., min-max scaling). Source of background map: Esri, HERE, Garmin, USGS, NGA.

ID	East (m)	North (m)	Threshold	EI	Area
1	**527189**	**6075536**	**6.00**	**0.34**	
2	527325	6075327	5.83	0.25	
3	527486	6074579	5.81	0.25	
4	527989	6073819	6.01	0.34	
5	528170	6072308	5.89	0.28	
6	527882	6072112	5.77	0.23	
7	528113	6072269	5.90	0.29	
8	529491	6074287	5.91	0.29	
9	531482	6075367	5.89	0.28	
10	531661	6075224	5.83	0.25	
11	532347	6075428	5.96	0.32	
12	532505	6075800	5.97	0.32	
13	533561	6076784	5.98	0.33	Flensburg Bay
14	533953	6077052	5.97	0.32	
15	534280	6077535	5.85	0.26	
16	535011	6078034	5.98	0.33	
17	535294	6078227	5.98	0.33	
18	535747	6078537	5.78	0.23	
19	536028	6078985	5.98	0.33	
20	536197	6079355	5.78	0.23	
21	536426	6079765	5.84	0.26	
22	537304	6080110	5.82	0.25	
23	537363	6080150	5.80	0.24	
24	537423	6080696	5.95	0.31	
25	**537662**	**6081369**	**5.97**	**0.32**	
26	538616	6081508	5.99	0.33	
27	539029	6081290	6.00	0.34	
28	539265	6081204	6.00	0.34	
29	539138	6080619	5.83	0.25	
30	538719	6080078	6.06	0.37	
31	538363	6079580	6.00	0.34	
32	538131	6078911	6.15	0.41	
33	538141	6078153	6.24	0.46	
34	538153	6077646	6.22	0.45	
35	538339	6077262	6.22	0.45	
36	538527	6076877	6.01	0.34	
37	538774	6076534	6.14	0.41	
38	539319	6076146	6.11	0.39	
39	539616	6076101	6.10	0.39	
40	539673	6076143	6.10	0.39	
41	540923	6076019	6.25	0.46	
42	541348	6075811	5.92	0.30	
43	541844	6075395	6.23	0.45	
44	542029	6075271	6.05	0.36	
45	542272	6075192	5.73	0.21	
46	543478	6075061	6.36	0.51	
47	544283	6074626	6.39	0.53	
48	545092	6074198	6.39	0.53	
49	545280	6074081	6.38	0.52	
50	**545469**	**6073964**	**6.35**	**0.51**	
51	546702	6073617	6.34	0.50	
52	547253	6073531	6.37	0.52	
53	547748	6073399	6.37	0.52	
54	548243	6073270	6.38	0.52	
55	548797	6073191	6.42	0.54	
56	549620	6072799	6.22	0.45	
57	550141	6072424	6.15	0.41	
58	551368	6072391	6.51	0.59	
59	551335	6072085	6.47	0.57	
60	551417	6071879	6.48	0.57	
61	551664	6071261	6.46	0.56	
62	551944	6070949	6.45	0.56	
63	552224	6070639	6.41	0.54	
64	552504	6070331	6.38	0.52	
65	552974	6069931	6.35	0.51	
66	553426	6069554	5.59	0.14	
67	553676	6069287	6.28	0.48	
68	553961	6068655	6.23	0.45	
69	554161	6068445	6.04	0.36	
70	554454	6068356	6.22	0.45	
71	554790	6068333	6.20	0.44	
72	555545	6067663	6.12	0.40	
73	555621	6067586	6.09	0.38	
74	555878	6067540	5.95	0.31	
75	**556033**	**6068141**	**6.13**	**0.40**	
76	556246	6068798	6.14	0.41	
77	556259	6069115	6.15	0.41	
78	556715	6069867	5.96	0.32	
79	557298	6070277	5.93	0.30	
80	557524	6070496	5.90	0.29	
81	557580	6070550	6.09	0.38	
82	557673	6070795	5.86	0.27	
83	557717	6071318	5.87	0.27	
84	557747	6071516	5.87	0.27	
85	557762	6072074	5.89	0.28	
86	559041	6072933	6.62	0.64	
87	559579	6072493	6.55	0.61	
88	559857	6072324	6.57	0.62	
89	560202	6072091	6.56	0.61	
90	560642	6071529	6.55	0.61	
91	560929	6071242	6.53	0.60	
92	561479	6070931	6.37	0.52	
93	561857	6070443	5.99	0.33	
94	561962	6070112	6.41	0.54	
95	562256	6069827	6.51	0.59	
96	562719	6069271	6.43	0.55	
97	562869	6069129	6.86	0.76	
98	563285	6068516	6.44	0.55	
99	563392	6067869	6.46	0.56	
100	**563405**	**6067422**	**6.87**	**0.76**	

ID	East (m)	North (m)	Threshold	EI	Area
101	563444	6066844	6.48	0.57	
102	563541	6066325	6.82	0.74	
103	563483	6065628	6.74	0.70	
104	563588	6065427	6.80	0.73	
105	563721	6065096	6.83	0.75	
106	563935	6064693	6.54	0.60	
107	564181	6064161	6.83	0.74	
108	564535	6063748	6.85	0.75	
109	564758	6063347	6.83	0.75	
110	564953	6063076	6.54	0.60	
111	565283	6062794	6.83	0.75	
112	565614	6062514	6.51	0.59	
113	566030	6062165	6.86	0.76	
114	566448	6061817	6.58	0.62	
115	566785	6061540	6.90	0.78	
116	567436	6060607	6.61	0.64	
117	567509	6060347	6.65	0.66	
118	567554	6059518	7.02	0.84	
119	566712	6058815	6.82	0.74	
120	566658	6058567	6.76	0.71	Schleimünde
121	566915	6058170	6.93	0.79	
122	566676	6057684	6.86	0.76	
123	566622	6057248	6.82	0.74	
124	566837	6056415	5.90	0.29	
125	**566790**	**6056167**	**6.88**	**0.77**	
126	566743	6055731	6.84	0.75	
127	566699	6055106	6.85	0.75	
128	566702	6054728	6.84	0.75	
129	566845	6054151	6.91	0.78	
130	566855	6053583	6.94	0.80	
131	566863	6053204	6.94	0.80	
132	566878	6052634	6.97	0.81	
133	566751	6052264	6.93	0.79	
134	566675	6051764	6.64	0.65	
135	566602	6051263	6.92	0.79	
136	566575	6050823	6.90	0.78	
137	566560	6050194	6.90	0.78	
138	566582	6049815	5.83	0.25	
139	566563	6049377	6.94	0.80	
140	566504	6048881	5.89	0.28	
141	566547	6048316	5.73	0.21	
142	566537	6047882	6.61	0.64	
143	566529	6047448	6.96	0.81	
144	566543	6046829	6.56	0.61	
145	566541	6046398	6.95	0.80	
146	566563	6045781	7.00	0.83	
147	566566	6045350	6.99	0.82	
148	566492	6044804	6.63	0.65	
149	566110	6044470	6.60	0.63	
150	**565727**	**6044137**	**6.63**	**0.65**	
151	565671	6043835	5.66	0.17	
152	565374	6043183	6.66	0.66	
153	565214	6042951	6.86	0.76	
154	565038	6042471	6.88	0.77	
155	564781	6041872	6.48	0.57	
156	564272	6041360	5.80	0.24	
157	564111	6041126	6.51	0.59	
158	563975	6040702	6.43	0.55	
159	563317	6040206	5.60	0.14	
160	563048	6040047	6.52	0.59	
161	562779	6039888	6.49	0.58	
162	562238	6039572	6.20	0.44	
163	561967	6039414	6.40	0.53	
164	561382	6039041	6.45	0.56	
165	560132	6038425	6.30	0.49	
166	559465	6038182	6.06	0.37	
167	559141	6037960	6.28	0.48	
168	558814	6037736	6.11	0.39	
169	558196	6037344	6.31	0.49	
170	557907	6037176	6.07	0.37	
171	557305	6037042	6.10	0.39	
172	556919	6036746	6.20	0.44	
173	556467	6036593	6.21	0.44	Eckernförde Bay
174	556059	6036502	6.04	0.36	
175	**555587**	**6036558**	**5.99**	**0.33**	
176	555005	6036698	5.97	0.32	
177	554532	6036757	5.92	0.30	
178	554526	6036063	6.16	0.42	
179	554604	6035705	6.30	0.49	
180	554922	6034970	6.32	0.50	
181	554986	6034822	6.35	0.51	
182	555340	6034362	6.48	0.57	
183	555565	6034197	6.50	0.58	
184	555998	6034079	6.30	0.49	
185	556430	6033963	6.35	0.51	
186	557003	6034044	6.19	0.43	
187	557415	6034142	6.16	0.42	
188	557985	6034226	6.11	0.39	
189	558461	6034181	6.11	0.39	
190	558620	6034167	6.18	0.43	
191	559119	6034398	6.14	0.41	
192	559659	6034693	6.02	0.35	
193	559950	6034872	5.98	0.33	
194	560171	6035191	NA	NA	
195	560900	6035528	6.40	0.53	
196	561381	6035749	5.36	0.02	
197	561577	6035797	5.31	0.00	
198	562164	6035939	6.54	0.60	
199	562900	6036066	6.56	0.61	
200	**563398**	**6036085**	**6.54**	**0.60**	

ID	East (m)	North (m)	Threshold	EI	Area
201	563822	6036239	5.33	0.01	
202	564125	6036212	6.38	0.52	
203	564619	6036232	6.18	0.43	
204	564928	6036459	6.45	0.56	
205	565686	6036648	6.35	0.51	
206	566146	6037114	6.64	0.65	
207	566484	6037150	6.45	0.56	
208	566970	6037176	6.41	0.54	
209	567494	6037264	6.38	0.52	
210	568018	6037354	6.70	0.68	Eckernförde Bay
211	568540	6037446	6.59	0.63	
212	569210	6037532	6.67	0.67	
213	569396	6037584	6.33	0.50	
214	570026	6037614	6.63	0.65	
215	570581	6037775	6.67	0.67	
216	570951	6037883	6.69	0.68	
217	571651	6038042	6.41	0.54	
218	572018	6038152	6.51	0.59	
219	572348	6038203	6.81	0.74	
220	573117	6038241	5.63	0.16	
221	573631	6038104	6.57	0.62	
222	573963	6037910	6.62	0.64	
223	574372	6037592	6.97	0.81	
224	574817	6037337	6.63	0.65	
225	**575264**	**6037084**	**6.61**	**0.64**	
226	575746	6036894	6.69	0.68	
227	576317	6036334	6.99	0.82	
228	576429	6036272	7.02	0.84	
229	576971	6035652	6.97	0.81	
230	577198	6035529	6.95	0.80	
231	577425	6035407	6.95	0.80	
232	578121	6034793	6.77	0.72	
233	577737	6033790	6.81	0.74	
234	577703	6033727	6.81	0.74	
235	577057	6033344	6.23	0.45	
236	576706	6032965	6.10	0.39	
237	576340	6032838	5.98	0.33	
238	575988	6032460	5.87	0.27	
239	575887	6032272	5.82	0.25	
240	576069	6031771	5.84	0.26	
241	576320	6031395	5.72	0.20	
242	576808	6030896	6.48	0.57	
243	577504	6030213	5.53	0.11	
244	577567	6029459	6.47	0.57	
245	577393	6028823	6.31	0.49	
246	577414	6028569	5.91	0.29	
247	577425	6027994	5.34	0.01	
248	577447	6027737	6.27	0.47	
249	577006	6027466	5.98	0.33	
250	**576197**	**6027378**	**5.98**	**0.33**	
251	576163	6027312	5.99	0.33	
252	575488	6026896	5.99	0.33	
253	575383	6026692	5.81	0.25	
254	575502	6026024	5.98	0.33	
255	575325	6025677	5.93	0.30	
256	575146	6025328	5.93	0.30	
257	574253	6023278	6.00	0.34	
258	574378	6023214	5.91	0.29	
259	574629	6023087	5.91	0.29	
260	575113	6022483	6.12	0.40	
261	575222	6022070	6.08	0.38	
262	574956	6021217	5.97	0.32	Kiel Bay
263	574885	6021073	5.97	0.32	
264	574849	6021001	5.90	0.29	
265	573843	6018646	5.93	0.30	
266	576517	6022147	5.96	0.32	
267	576461	6022353	5.97	0.32	
268	576666	6024031	6.02	0.35	
269	576876	6024456	6.12	0.40	
270	577525	6024834	5.87	0.27	
271	577559	6024903	6.06	0.37	
272	577607	6025311	6.07	0.37	
273	577755	6025919	6.02	0.35	
274	578055	6026525	6.16	0.42	
275	**578577**	**6027579**	**5.77**	**0.23**	
276	578778	6028286	5.62	0.15	
277	578913	6028859	5.72	0.20	
278	579009	6029051	5.86	0.27	
279	579025	6029680	5.46	0.07	
280	579344	6030317	6.21	0.44	
281	579772	6030581	6.54	0.60	
282	580144	6031032	6.45	0.56	
283	580985	6031252	6.48	0.57	
284	581666	6031157	6.67	0.67	
285	581932	6031107	6.60	0.63	
286	582112	6031179	6.56	0.61	
287	582502	6031386	6.53	0.60	
288	583385	6031123	5.95	0.31	
289	583313	6032180	5.76	0.22	
290	583552	6032380	6.27	0.47	
291	584174	6032789	6.37	0.52	
292	584818	6032953	6.79	0.73	
293	585285	6033046	6.81	0.74	
294	585577	6033065	6.79	0.73	
295	586333	6033181	6.42	0.54	
296	586855	6033097	6.54	0.60	
297	587610	6032911	6.52	0.59	
298	587988	6032819	6.92	0.79	
299	588454	6032613	6.52	0.59	
300	**588805**	**6032459**	**6.94**	**0.80**	

ID	East (m)	North (m)	Threshold	EI	Area
301	589419	6032270	6.57	0.62	
302	589889	6032068	6.95	0.80	
303	590151	6032032	6.53	0.60	
304	590950	6031620	6.41	0.54	
305	591159	6031456	6.50	0.58	
306	591672	6031017	6.54	0.60	
307	591977	6030741	6.64	0.65	
308	592402	6030417	6.64	0.65	
309	592829	6030095	6.88	0.77	
310	593285	6029839	6.39	0.53	
311	593646	6029697	6.91	0.78	
312	594225	6029396	6.53	0.60	
313	594660	6029078	6.90	0.78	
314	594904	6028986	6.57	0.62	
315	595439	6028558	6.91	0.78	
316	595782	6028355	6.57	0.62	
317	596272	6028174	6.47	0.57	
318	596740	6027927	6.90	0.78	
319	597234	6027749	6.40	0.53	
320	597628	6027681	6.40	0.53	
321	598000	6027549	6.60	0.63	
322	598520	6027440	6.89	0.77	
323	599017	6027266	6.48	0.57	
324	599516	6027094	6.89	0.77	
325	**600039**	**6026990**	**6.91**	**0.78**	
326	600518	6026755	6.89	0.77	
327	600873	6026562	6.50	0.58	
328	601356	6026329	6.90	0.78	
329	601840	6026098	6.89	0.77	
330	602199	6025908	6.45	0.56	
331	602708	6025746	6.48	0.57	
332	603218	6025585	6.88	0.77	
333	603602	6025465	6.89	0.77	
334	604094	6025240	6.87	0.76	
335	604697	6024910	6.48	0.57	
336	605044	6024659	6.42	0.54	
337	605522	6024371	6.87	0.76	
338	605762	6024228	6.87	0.76	
339	606374	6023904	6.40	0.53	
340	606800	6023417	5.92	0.30	
341	607005	6023140	6.46	0.56	
342	607399	6022518	6.56	0.61	
343	607418	6022075	6.75	0.71	
344	607609	6021730	5.93	0.30	
345	607838	6021522	6.66	0.66	
346	608317	6021173	6.27	0.47	
347	608682	6020929	6.45	0.56	
348	609067	6020755	6.39	0.53	
349	609616	6020103	6.35	0.51	
350	**609563**	**6019899**	**6.65**	**0.66**	
351	609764	6019557	6.28	0.48	
352	610359	6019045	6.29	0.48	
353	610768	6018942	6.73	0.70	
354	611332	6018875	5.46	0.07	
355	611640	6018944	6.71	0.69	Hohwacht Bay
356	612116	6019117	6.71	0.69	
357	612593	6019290	6.76	0.71	
358	613052	6019397	6.76	0.71	
359	613616	6019337	6.78	0.72	
360	614150	6019142	6.80	0.73	
361	614578	6019117	6.37	0.52	
362	615022	6019160	6.26	0.47	
363	615495	6019342	5.87	0.27	
364	615816	6019486	6.30	0.49	
365	616136	6019631	6.73	0.70	
366	616804	6020059	6.27	0.47	
367	616985	6020234	6.39	0.53	
368	617332	6020517	6.75	0.71	
369	617678	6020800	5.91	0.29	
370	618024	6021082	5.91	0.29	
371	618546	6021540	6.27	0.47	
372	618903	6021890	6.28	0.48	
373	619272	6022307	6.21	0.44	
374	619585	6022455	6.16	0.42	
375	**619830**	**6022967**	**6.27**	**0.47**	
376	620195	6023387	6.77	0.72	
377	620547	6023740	6.76	0.71	
378	620897	6024095	6.25	0.46	
379	621086	6024342	6.35	0.51	
380	621462	6024840	6.82	0.74	
381	621945	6025178	6.38	0.52	
382	622413	6025450	6.34	0.50	
383	622747	6025750	6.86	0.76	
384	623321	6025862	6.79	0.73	
385	623774	6026071	6.39	0.53	
386	624239	6026353	5.56	0.12	
387	624436	6026686	6.73	0.70	
388	624620	6026947	6.75	0.71	
389	625133	**6027519**	6.74	0.70	
390	625461	6027829	6.83	0.75	
391	626172	6027998	6.78	0.72	
392	626472	6028166	6.44	0.55	
393	626893	6028241	6.41	0.54	
394	627566	6028202	6.76	0.71	
395	627963	6028138	6.34	0.50	Heiligenhafen
396	628240	6028167	6.34	0.50	
397	628914	6028133	6.32	0.50	
398	629456	6028123	6.29	0.48	
399	629589	6028103	6.67	0.67	
400	**630428**	**6028266**	**6.64**	**0.65**	

ID	East (m)	North (m)	Threshold	EI	Area
401	630959	6028190	6.27	0.47	
402	628995	6026884	5.96	0.32	
403	629397	6026824	5.96	0.32	
404	629542	6026875	5.96	0.32	
405	630998	6026520	5.91	0.29	Heiligenhafen
406	631123	6026430	5.74	0.21	
407	631402	6026465	5.89	0.28	
408	631959	6026536	6.21	0.44	
409	632401	6026768	6.31	0.49	

ID	East (m)	North (m)	Threshold	EI	Area
501	625716	5997766	6.37	0.52	
502	625337	5997281	6.98	0.82	
503	624947	5996723	7.02	0.84	
504	624761	5996519	6.22	0.45	
505	624529	5995945	6.96	0.81	
506	624173	5995688	6.88	0.77	
507	623780	5995136	5.85	0.26	
508	623592	5994934	5.89	0.28	
509	622705	5994368	5.64	0.16	

Table A1: Location ID, spatial coordinates East and North, defined threshold value and the EI along the SH coast. For clarity, different regions are marked, which are indicated in Figure 8.

View publication stats